NTNU
Norwegian University of
Science and Technology

Design and testing of Flux Switched Permanent Magnet (FSPM) Machines

Njål Rotevatn

Master of Science in Energy and Environment
Submission date: June 2009
Supervisor: Robert Nilssen, ELKRAFT

Norwegian University of Science and Technology
Department of Electrical Power Engineering

Problem Description

The novel Flux Switching concepts for Permanent Magnet machines are to be investigated in terms of a theoretical survey of relevant literature and by building a prototype for practical evaluation of the concepts. The main academic focus of the work is the planning of the machine and laboratory instrumentation setup and the testing/evaluation of relevant parameters. The machine is to be tested as a generator with a passive load.

The student must choose a prototype design and order parts such as magnets and lamination in cooperation with the Workshop at NTNU. Planning of the assembly and the building of a lab testing jig is also a part of this work.

In order to give a good validation of the machine, the student must present analysis results focusing on flux densities and flux switching sequences. These theoretical results are expected to be the basis for laboratory oriented experiments with resistive and capacitive loading of the machine, where machine parameters such as induced voltage, inductances, losses and efficiency are determined.

Assignment given: 02. February 2009
Supervisor: Robert Nilssen, ELKRAFT

Design and testing of Flux Switched Permanent Magnet (FSPM) Machines

Njål Rotevatn

***Abstract*—This thesis offers a short overview of the most important stator mounted permanent magnet machines, with a closer look on the FSPM design. A FSPM machine have been built and tested as a generator, to get a better understanding of the machine concept.**

The focus of the work have been on the well documented 12/10 (Stator teeth/ Rotor teeth) design while the novel 12/14 pole design have also been tested, as a rotor change is the only difference between the two designs.

The machine have been simulated in COMSOL, where inductances, back emf and cogging have been found and compared with the measured results.

***Index Terms*—FSPM, Electrical machine, PM.**

I. Introduction

BRUSHLESS permanent magnet machines are usually designed with magnets in the rotor, rotor-PM machines. In recent years there have however been much research on machines with the magnets mounted in the stator, stator-PM machines.

Stator mounting of the PMs mainly give two advantages: The heat sensitive magnets can more easily be cooled, and the magnets will not be subjected to the centrifugal forces of a spinning rotor. Several designs exists for stator-PM machines, where the DSPM (Doubly salient permanent magnet) and the FRM (Flux reversal machine) are the most noteworthy together with the FSPM. They are all doubly salient machines where the rotor position determines the path of the stator magnet flux, and hence the stator coil flux coupling.

DSPM: The DSPM machine, Figure (2) have magnets mounted tangentially in the stator, with a phase number dependent set of stator teeth between them. This configuration give a trapezoidal back emf and have unipolar flux coupling in the stator coils. A comparison between FSPM and DSPM machines done in [1], concludes that the DSPM is inferior to the FSPM in terms of torque density, but have better cogging performance and higher torque per magnet volume.

FRM: The three phase FRM machine, Figure (3), was introduced in [2]. It has two surface mounted magnets at each stator tooth, a configuration that give a bipolar flux coupling, and a trapezoidal or sinusoidal back emf depending on the machine design. The FRM have magnets in the air gap, magnetically in series with the coils. This design give problems related to the fastening of the magnets as well as magnet eddy current losses. The series placement of the magnets will additionally contribute to higher air gap reluctance, and hence lower the machine inductances.

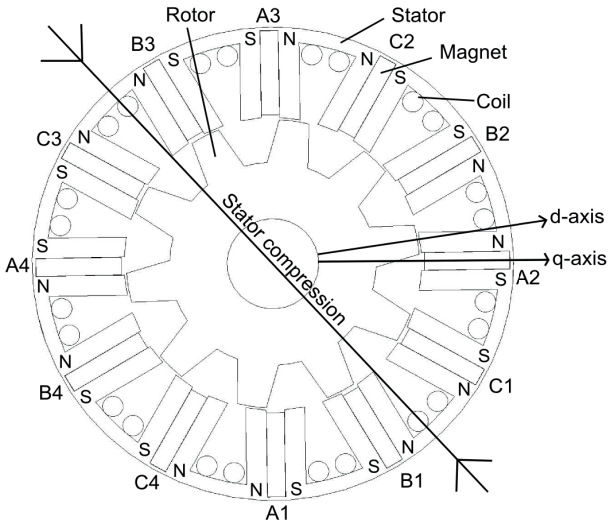

Figure 1. The 12/10 FSPM machine built for the thesis

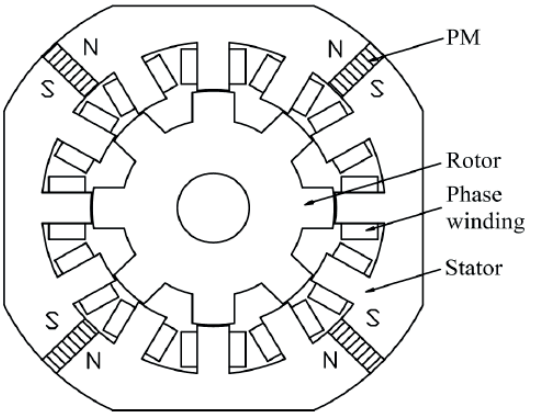

Figure 2. A 12/8 DSPM machine

FSPM: The FSPM principle was first proposed as a single phase machine [3], Figure (4), and have recently gained much interest with the polyphase designs introduced in [4], similar to the. The winding configuration of the 3-phase machines, Figure (1), is seen to have changed from that of the 1955 proposal, but the flux switching principle remains the same.

The FSPM machine is very similar to the DSPM machine in that it has tangentially placed magnets in the stator. The unique feature of the FSPM is that each winding is placed around a set of two stator teeth, with one tangentially placed magnet between them, this give bipolar flux linkage in the coils, similar to the FRM machine, but without the drawback

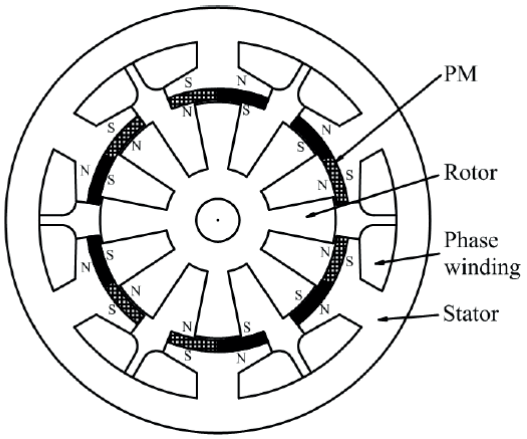

Figure 3. A 8/12 FRM machine

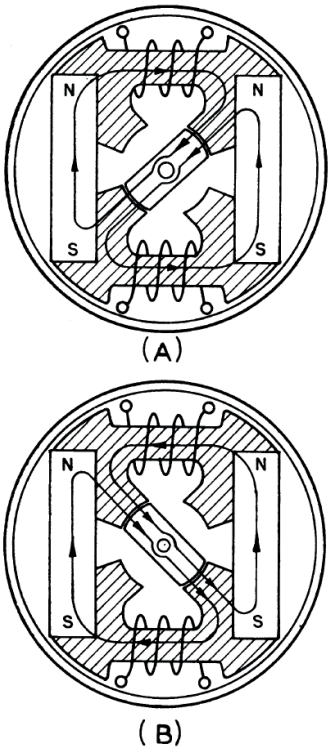

Figure 4. The first FSPM machine as introduced in 4

of surface mounted magnets. The back-emf of the three phase machines to be examined in this thesis is naturally sinusoidal, making them suitable for brushless AC.

A wide variety of alternative flux switching designs are presented in literature, they can not all be thoroughly presented in this paper, but a few examples are still presented, to show some of the possibilities of flux switching machines:

-Multi tooth FSPM machines, as they are presented in [5], [6], claims to both give higher torque and lower magnet than the conventional FSPM machine, at least at low current levels.

-Parallel Path Magnetic Technology (PPMT). [7] presents what appears to be FSPM machines with a winding layout similar to that of [3] under the name PPMT. These machines claim to be superior to most other machines, but the amount of advertisement in these claims are uncertain

-The FSPM design is proposed as an linear actuator in [8], an interesting design where the advantages of convectional linear tubular machines are combined with that of the FSPM design; No end windings and no magnets on the moving part, this facilitates easier magnet cooling and decouples the magnet volume from stroke length of the machine.

-Current exited flux switching machines for use in power tools are presented in [9]. The design removes the need for brushes used in the common universal machines, and is claimed to be very cost effective. Black and Decker have according to the paper actually launched a flux switching based tabled saw on the design.

II. FSPM operating principles and important parameters

A. The flux switching sequence

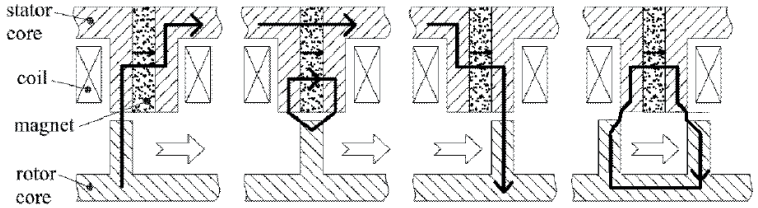

Figure 5. The flux switching principle

The flux switching sequence of a FSPM machine can be seen in Figure (5). It is seen how the flux in each stator tooth is unipolar, while the combination of two stator teeth in each stator pole give a bipolar coil flux coupling, switching direction with rotor position. The figure explains the principle behind flux switching well, but in practice with the number of stator poles $\neq$ the number of rotor poles it is fairly complicated to determine the exact flux switching sequence, as it is an interplay between all the stator rotor air gaps. It should also be observed that there will be some leakage flux between the stator teeth inside each pole, this will obviously be more significant if the rotor poles are wide, and if the number of rotor poles$>$ the number of stator poles.

B. Number of stator poles

A simple but important factor of rotating FSPM machines are that the number of stator teeth must always be an even number, as stator magnets must alternate in magnetization direction. In a circular setup in a rotating machine this requires an even number of poles.

C. Fundamental frequency

One electrical period of an FSPM machine is equal to the time it takes for the position of a rotor tooth at the start of a period to be filled by the next tooth, thus putting the machine into the same magnetic state as it was at the beginning of the period, similar to a rotor-PM machine, but without pole polarity. The number of electrical periods per mechanical revolution of the machine is therefore equal to the number of rotor teeth, giving the electrical frequency $f_e = \frac{N_r \times rpm}{60}$.

D. Radial forces

The magnetically forces in a FSPM machine will always pull radially on the rotor teeth. The sum of these forces are desired to be as low as possible, and at particularly to not oscillate in direction or strength, as this will induce vibrations with negative effects on machine durability, in particularly bearing life. A simple way of removing the radial forces is choose a machine where N_r (number of rotor teeth) and N_s (number of stator teeth) have a common factor larger than one. Such machines will have comparatively higher fundamental frequencies, making them less suited for high speed operation, as the fundamental frequency is an important part of the losses in an electrical machine, [10] examines a 5/6 FSPM machine with particular focus on radial forces.

E. Cogging torque and skewing

The cogging torque in a rotating electrical machine can be expressed as $T(\theta) = \frac{dW(\theta)}{d\phi(\theta)}$ where W is the magnetic energy in the machine, and ϕ is the angular position of the rotor. The calculation of these forces requires detailed modeling of the machine. The number of cogging periods per electrical period is however easy to find and is equal $N_s/HCF(N_s \,\&\, N_r)$ where HCF is the highest common factor. This give a cogging frequency $f_c = \frac{N_r \times N_s}{HCF(N_s \,\&\, N_r)} \frac{rpm}{60}$. These relations are easily verified by observing how each electrical period of the machine give the specified number of equal magnetic energy states.

The rotor of an FSPM machine are usually made of steel laminations, this means that it can easily be skewed by angulary displacing the lamination sheets. The effect of skewing is that of an moving average filter, and can generally be expressed as $g(x) = \frac{1}{Y}\int_0^Y f(x+y)dy$, where $f(x)$ is the function of the variable is question before skewing, x is the position, Y is the skewing and $g(x)$ is the resulting function after skewing. For $f(x) = sin(x)$, such as the fundamental component of the back emf, this can be shown to become $g(x)$=$\frac{cos(x+0)-cos(x+Y)}{Y}$. From this it can be seen that skewing equal to the length of one cogging period will completely remove cogging, while the effect on the fundamental component of the back emf will be small if f_c sufficiently much larger than f_e. [11] Examines the effect of skewing for a 6/5 and 6/4 FSPM, skewing apparently shows favorable results for the harmonics content of the back emf as well as for the cogging.

F. Torque equations

The torque equations of 3-phase synchronous machines are best described by examining the machine in a dq reference frame. Phase values are transformed to dq values by Equations (1-3).

$$W = \frac{2}{3}\begin{bmatrix} 1/\sqrt{3} & 1/\sqrt{3} & 1/\sqrt{3} \\ cos(\phi) & cos(\phi - \frac{2\pi}{3}) & cos(\phi - \frac{4\pi}{3}) \\ sin(\phi) & sin(\phi - \frac{2\pi}{3}) & sin(\phi - \frac{4\pi}{3}) \end{bmatrix} \quad (1)$$

$$\begin{bmatrix} i_0 \\ i_d \\ i_q \end{bmatrix} = W \times \begin{bmatrix} i_a \\ i_b \\ i_c \end{bmatrix} \quad (2)$$

$$\begin{bmatrix} v_0 \\ v_d \\ v_q \end{bmatrix} = W \times \begin{bmatrix} v_a \\ v_b \\ v_c \end{bmatrix} \quad (3)$$

Machine torque can than be found by Equation (4), where

$$T = \frac{3}{2}N_r(\lambda_{pm} i_q + (L_d - L_q) i_d i_q) \quad (4)$$

Where λ_{pm} is the PM flux linkage. Reluctance torque in FSPM machines are negligible, and the equation can be reduced to:

$$T = k_T i_q \quad (5)$$

where $k_T$is the torque constant $k_T = \frac{3}{2}N_r\lambda_{pm}$, alternatively $k_T = \frac{3v_q}{2\omega_m}$, at an unloaded machine, where v_q equals the peak value of the per phase back emf E_f, easily measured at the terminals of an unloaded machine.

III. Choice of FSPM geometry

Several geometries where examined such as 5/6, 11/12 and 13/12 layout. The 11/12 and 13/12 layout was found to promising for a setup with only every other stator pole wound as covered in [12], [13]. The 5/6 machine would be fairly simple to make with only 6 stator teeth, and would be suited for high speed, as it have a low fundamental frequency. All the these designs are however magnetically unbalanced, an extra factor that would have had to be considered if one of these machines where built.

The geometry finally chosen for the prototype machine is a 12 pole stator with a changeable rotor of 10 or 14 poles.

The 12/10 configuration is well covered in literature such as [14], [15], [10], [1], [16], [4] and more. It has balanced radial magnet forces from symmetry, thus making it a suitable introduction to FSPM machine design.

The 12/14 was chosen in order run an initial test on this promising geometry. The idea is that the relatively higher fundamental frequency of a 14 pole rotor will give 40% higher torque than a 10 pole rotor at the same λ_{pm} (Equation (4)).

The 12/10 and 12/14 machines have similar stator layout with the only difference being that the 14 pole machine have negative phase sequence when compared with the 10 pole machine. The only major operation in changing from the 12/10 to the 12/14 layout is therefore the rotor change.

A. Machine optimization theory

The main focus of the thesis was to build and test a FSPM machine prototype, the time spent optimizing the design would therefore have to be limited. The principles of [15], [14], as well as some qualitative results from the lumped parameter model developed was used to decide the layout of the machine. With fem analysis used mainly to confirm that the chosen design was reasonable with respect to cogging torque and voltage waveforms. Only the 12/10 machine was considered in the optimization, as time was limited.

FSPM optimization as covered in literature, and used in this thesis, is based on what might be called the reference design

where magnets, stator teeth, winding slots as well as rotor teeth and back iron that are all of the same width[1].

The relationship between these variables as well as the air gap length and inner-/outer stator diameter fully defines the machine 2D layout (as long as alternative magnet and rotor-/stator teeth shapes are disregarded). The main geometric relations important for FSPM machine performance are:

-Magnet-/Slot width vs stator tooth width. The magnets, winding slots and stator teeth in an FSPM machine are evenly spaced to achieve symmetry, this means that a increase in stator tooth width, means an equal decrease in magnet- and winding slot width. Changes in this variable is a trade off between flux path reluctance and magnet-/copper volume. [15] say that the stator teeth should be equal to that of the magnet width, while [14] concludes that the stator teeth should be widened approximately 10% when the rotor tooth with are examined together with the rotor tooth width.

-Back iron width. Leakage flux as well as the fact that the flux in the stator teeth have two back iron paths, one form each neighboring pole, to divide into. Back iron flux density is therefore lower that that in the stator teeth, a decrease in back iron width, bringing the back iron closer to saturation will allow for more copper at the same outer diameter. A reduction to 70% of the original value is prescribed in [15]

-Magnet back iron bridge. It is possible to have a small bridge between the stator segments, allowing the stator to be produced in one piece easing the production of the machine. This will have a negative effect on machine performance, this is covered in [15].

-Split ratio, outer/inner stator diameter. As with all machines there is a balancing between inner stator diameter, as these decide the torque arm and the torque producing area of a machine, as well as the copper volume, and in FSPM machines also the magnet area.

-Rotor teeth width. The rotor tooth width is important in the determination of the machine back emf, as it influences the flux switching timing and the reluctance of the flux path. 1.46 times the base value is prescribed in [15].

1) Final 12/10 Design: The final design specifications is listed in Table (I). The chosen machine design have rotor-/stator diameters of a little more than twice that of the machines in [15], [14], but the air gap in the chosen machine design is doubled as well, meaning that flux density and the shape of the back emf should be similar to that of the mentioned papers. The split have also been chosen to be similar to the smaller machines, this choice is however somewhat questionable. A machine whose diameter is doubled, with all other parameters kept the same, as is approximately the case with the machine in question, will need double the number of ampere turns to keep the flux density contribution from the windings at the same level. The copper area in the same machine will however grow with the square of the diameter, giving ~twice the flux contribution from the windings per Ampere than that of the smaller machine.

[1]This is a small lie since the stator teeth are not pointing directly towards the center of the machine, they are instead in parallel with the magnets. The stator teeth are hence cut at an angle in the air gap, giving a stator tooth air gap width that is different (1% in 12 poled stator) from the stator tooth width.

Table I
MACHINE SPECIFICATIONS

Number of phases	3
Number of stator teeth	12
Number of rotor poles	$10/14$
Outer diameter of stator	$210mm$
Inner diameter of stator	$129.87mm$
Air gap length	$1mm$
Active axial length	$50mm$
Number of turns per pole	174
Magnet remanence	$1.16T$
Magnet relative permeability	1.05
Copper fill factor	0.5
Rated Torque	28
Rated speed	$400rpm$
Rotor tooth width top/bottom	13/18mm
Stator back iron width	6.3mm
Stator tooth width	8.91mm
Magnet width	8mm
Rotor tooth height	18.3mm
Stator support bridge	$1.5mm$

Machine volume and mass are listed in Table (II). The machine volume is somewhat difficult to determine because of the end windings, and have been calculated as $1.2\pi R_s^2 L_a$, where R_s is outer stator diameter, L_a is the active length of the machine, giving the active volume of the machine plus 20% for end windings.

Table II
MASS AND VOLUME OF THE MACHINE

	Volume	Mass
Sheet steel 10 pole	$0.94dm^3$	$7.2kg$
Sheet steel 14 pole	$1.00dm^3$	$7.7kg$
Magnets	$0.175dm^3$	$1.3kg$
Copper	$0.33dm^3$	$2.9kg$
Total 10 pole	$2.1dm^3$	$11.9kg$
Total 14 pole	$2.1dm^3$	$11.5kg$

2) Final 12/14 Design: The 14 tooth rotor was made with the same dimensions as the 10 tooth rotor, as no optimization calculations had been performed on the 14 pole rotor. This design is however unlikely to be the best for the 14 pole rotor. One factor in particular is the leakage flux depicted in the last part, Figure (5), as this will lead to increased iron losses and probably lower back emf than the optimum rotor pole width.

IV. CONSTRUCTION

All parts where drawn in Solid Works, to get drawings for production purposes as well as visualization of the machine. Solid Works drawings are seen in Figure (6) and on the front page.

A. Stator

The stator stack where ordered fully assembled, leaving only the mounting of winding and magnets. The magnets where easily glued into their slots, but the stator became eccentric because the magnetic forces caused stator to shift so that all the clearance between magnets and the magnet slots ended up in two opposite stator slots. The general principle behind this is shown in Figure (7), while the orientation of this eccentricity

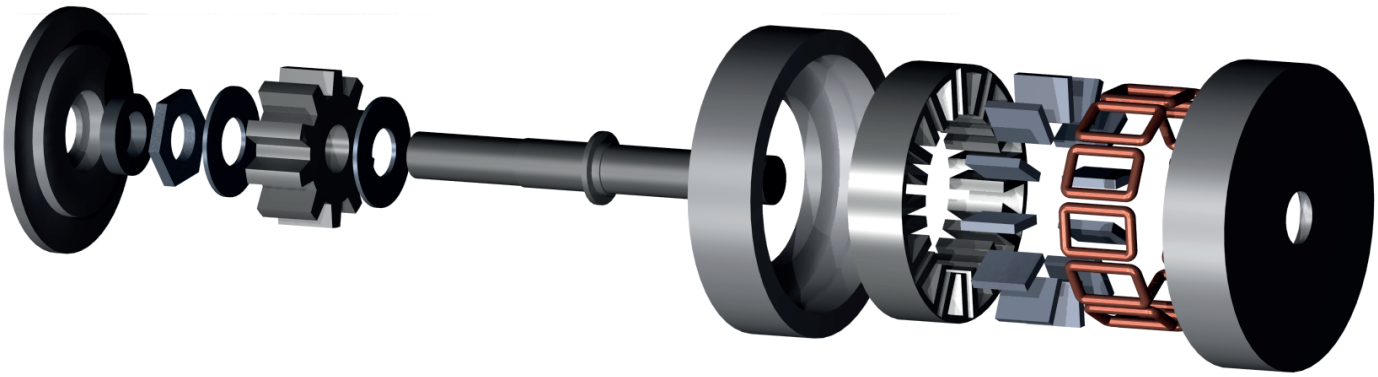

Figure 6. Exploded view of the machine

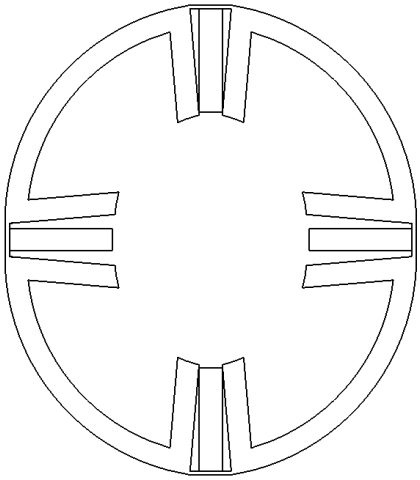

Figure 7. Figure showing mechanism behind machine eccentricity

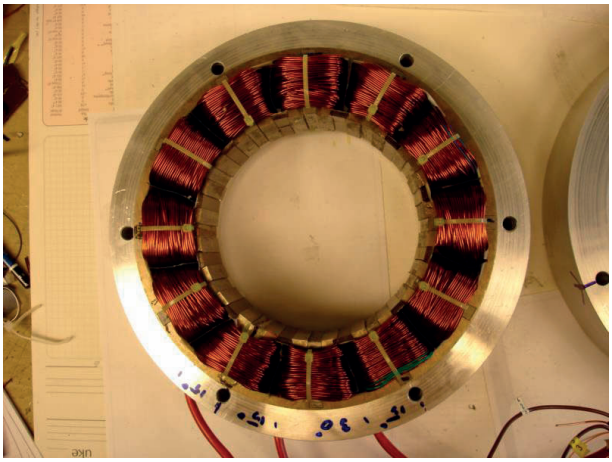

Figure 8. Wound stator

is shown on Figure (1). The air gap grew to ~1.2mm at the largest, and shrunk to about ~0.8 at the smallest, this is far from ideal, and could probably have been avoided by placing a mold into the stator center while the magnet glue dried, smaller clearances on magnet width vs. magnet slot width should also help.

The coils where fitted without major problems. Each coil was wound onto a mold, and then tread onto the stator pole. This posed some challenge, as the slot opening is smaller than the bottom width of the coil, but all coils where successfully mounted and secured with turbonit wedges in the slot openings, the stator is shown in Figure (8) .

Additional elements of the stators are search coils on pole B1 and B2. Thermal elements where placed inside the windings to monitor coil temperature, as the coils are assumed to be the hottest part of the machine.

B. Rotor

The lamination sheets where ordered unmounted as the possibility to skew the rotor where wanted. The fastening of the rotor sheets to the rotor shaft where where done by threading the shaft so the lamination sheets could be clamped together, with the desired skewing angle, by a screwing a nut onto the shaft (fig. 9).

C. Casing

The casing where designed lock onto the stator by clamping it at the back iron. It was constructed with a lid that allows the rotor to be changed without the unclamping of the rotor from the casing. Figure (10) show how the rotor mounting operation is done with the help of a lathe. Bearing housings where milled into the lid and the opposite half of the casing.

Holes drilled into the casing allow for possible air cooling. The holes where placed near the center of the shaft on the lid side of the casing and near the outside on the other side, to achieve a possible fan effect from the spinning rotor. The

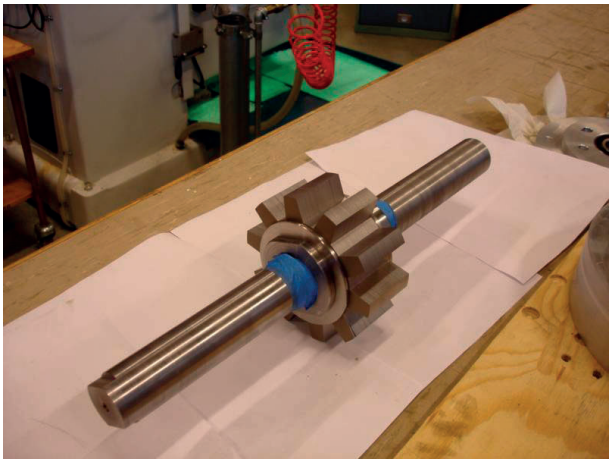

Figure 9. Picture of 10 pole rotor

holes where however closed up during testing, as the machine where not run long enough to get any significant temperature rise during testing.

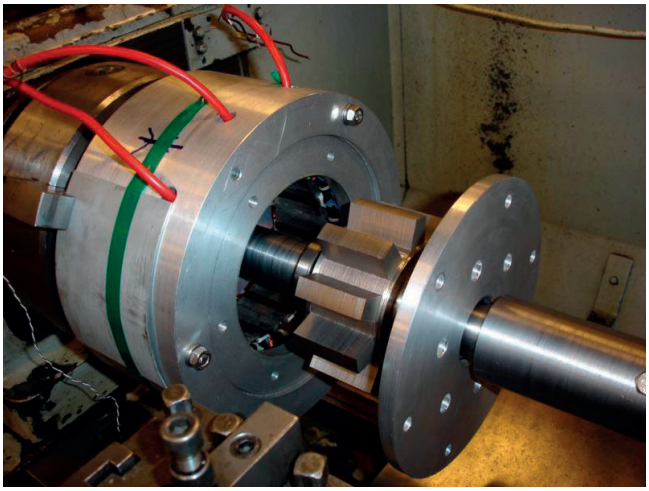

Figure 10. Mounting of rotor

D. Test rig

Dynamic test setup: The FSPM machine where mounted in a rig with a DC motor, while a torque sensor and a tachometer where used to get measurements of the generator input.

Locked rotor test setup: Locked rotor tests where performed by mounting a lever to the rotor shaft and controlling this lever, and thereby the rotor position, by turning a threaded rod fixed to the machine foundation and the lever Figure (11).

A removable brass rod where fixed to the rotor in the same position as a one of the rotor teeth, this enabled the rotor position to be read off a paper protractor fixed to the machine. A position encoder could have been used, but the solution with the protractor where thought to be accurate enough, while being much simpler to set up.

V. Simulation models

All electric machine design involves the determination of a great many largely interdependent variables. In the FSPM machine this is less intuitive than in a more conventional machine, as its the interplay of the varying reluctance of all the stator teeth air gaps that determines the flux path, and hence the back emf. The design process was therefore started with the development of a simple lumped parameter model of a general FSPM machine (Appendix I), a great tool in the understanding of the FSPM machine works. Comsol was used for further analysis of the machine, as further development of the lumped parameter model with inclusion of nonlinear magnetization parameters in the magnetic steel, fringing and leakage fluxes as is done in [14] would be beyond the scope of this thesis.

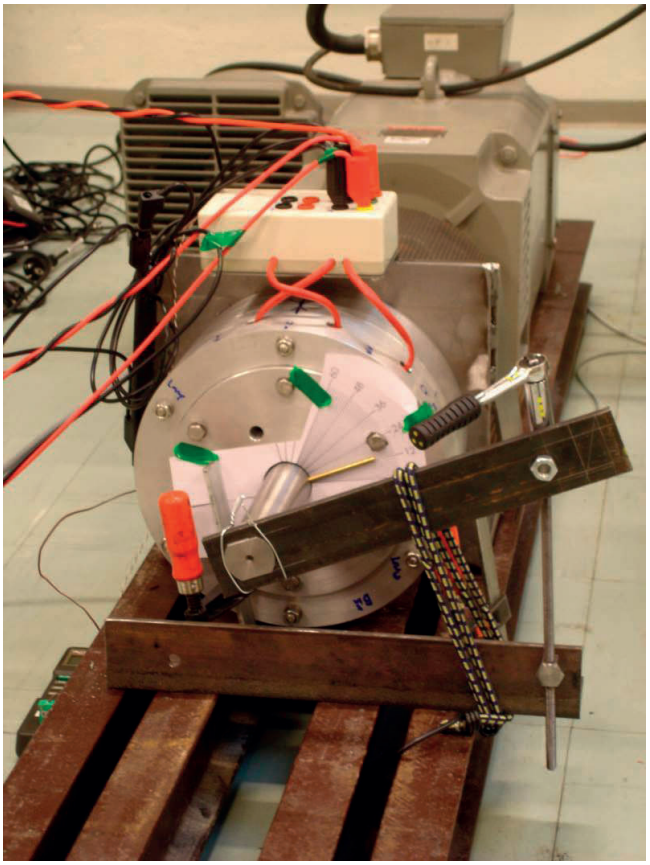

Figure 11. The setup for locked rotor testing

A. Lumped parameter model

A very simple approach was chosen for the model, namely air gaps modeled without fringing effects, and an infinitely permeable rotor. This give a machine model, as shown in Figure (12), where ϕs1 and Zm1 models the magnet, and Zs11 and Zs12 models the air gap permeance of the stator teeth in stator coil 1 etc. The model is easily scaled for any number of stator and rotor poles, simply by the input parameters of the simulations. By calculating the air gap permeances for the different rotor positions of a electrical period and solving the resulting matrix equations, the individual coil flux linkage waveforms is acquired and can be analyzed.

The lack of saturation modeling resulted in magnetic flux densities of several Tesla for otherwise reasonable models, the

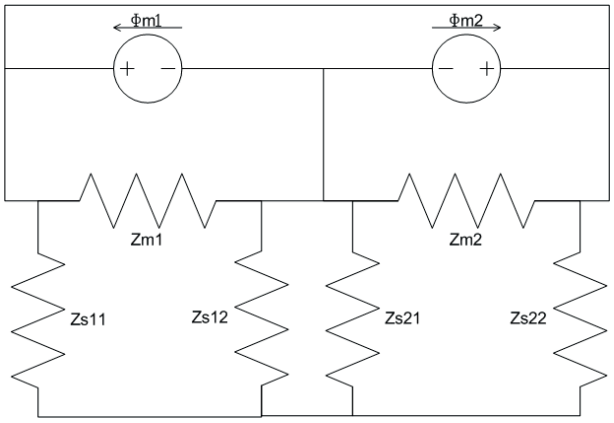

Figure 12. Lumped parameter model of FSPM with 2 stator teeth

model was however found to be very useful for qualitative examination of the FSPM concept, as parameters such as stator pole number, rotor pole number, rotor tooth width, stator tooth with etc. can all be easily varied by simply changing the input of the program . Figure (13) show coil flux linkages for a

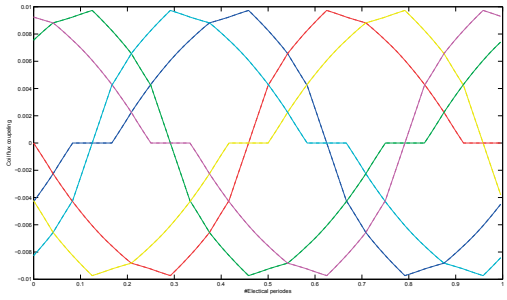

Figure 13. Coil flux coupling from 12/10 lumped parameter model

12/10 machine with rotor teeth 1.4 times stator teeth width.

B. FEM simulations

The importance of saturation- and fringing effects limited the usefulness of the lumped parameter model developed in the early phase of the project. COMSOL 3.5a have therefore been used for 2D FEM simulations of the machine, with main focus on back emf, inductances and cogging torque calculations.

Saturation effects are important in the FSPM machine, a H-B curve obtained from the producer of the sheet laminations, material M330-35A, have therefore been used. The drawings produced in Solid Works for the ordering of the machine steel laminations was exported to COMSOL, ensuring an accurate model. The entire machine have been simulated, although it should be possible to simulate only half the machine, as the machine is symmetric about a cut through the center. Work was however not put into this, as computing time and a computer with sufficient power and memory where available.

1) Back emf: The COMSOL - AC/DC unit for rotating machinery where used to simulate the machines with the rotor moving at 400 rpm. The back emf was calculated by integrating the induced voltage over the area of each conductor, dividing this value by the area, multiplying with the active machine length, and adding all these voltages together. Phase voltage per turn is obtained and multiplied with the number of turns to get the back emf.

2) Cogging: COMSOL contains functions for the calculation of torques and forces in a rotating machine, initial trials did however give strange results, an alternative approach examining the total magnetic energy of the machine, was therefore used.

The magnetic energy for the machine can easily be obtained from the simulations done for the back emf. A numerical derivation can then be done in Matlab, finding the cogging power, finally the cogging torque is found by the well known $T = P/\omega_m$. Some smoothing filters to fix up numerical noise was used before the results where plotted.

3) Inductances: The inductances in the machine where calculated by adding currents to the windings, and varying these sinusoidally in a transient simulation. The voltages induced in the windings where than calculated by the same method used for the back emf. The inductances varies with the rotor position, a Matlab script was therefore written to run the Comsol simulation for different rotor angles, recording applied currents and induced voltages for each step.

Self and Mutual inductances: Self and mutual inductances where calculated by adding a current to phase A, and recording the induced voltages for all the phases. The model does not include resistances, this give an inductive circuit where the inductances can easily be calculated by the frequency and peak-peak values of the voltage and current, as done in Equation (11) and (7). Fairly linear magnetic materials giving smooth symmetrical induced voltages are required to use the peak-peak values, this appears to be the case with the $1e6\,A/mm$ current value used in the simulations.

$$H_a = \frac{v_{a\,Pk-Pk}}{i_a\,Pk-Pk \times 2\pi f_e} \tag{6}$$

$$M_{ab} = \frac{-v_{b\,Pk-Pk}}{i_{a\,Pk-Pk} \times 2\pi f_e} \tag{7}$$

d- and q axis inductances: The FSPM machine are designed to run as an ac machine, the d- and q axis inductances are therefore interesting to calculate. This can be done by applying 3-phase currents to the machine for different positions, and than finding the dq currents and voltages through Equation (2) and (3).

Inductances are then fund as the same way as the self- and mutual inductances, by using Equations (8) and (9).

$$L_d = \frac{v_{d\,Pk-Pk}}{i_{d\,Pk-Pk} \times 2\pi f_e} \tag{8}$$

$$L_q = \frac{v_{q\,Pk-Pk}}{i_q\,Pk-Pk \times 2\pi f_e} \tag{9}$$

4) Simulation of an eccentric stator: The stator eccentricity that occurred during the building of the machine where included in some of the FEM simulation, as especially the cogging where a factor of concern. These inclusion of eccentricity where performed by compressing the stator 0.3% along the axis shown as stator compression on Figure(1) , while

the stator where stretched 0.3% along the perpendicular axis. The thought is that 0.3% compression and stretching should have little effect on the simulation results, other than the 20% change in the air gap length.

VI. Machine test setup

A. Dynamic testing

Dynamic testing where done with the machine and loads all wye connected, with mutually isolated neutral points.

Power from the drive motor where read off the torque transducer and the tachometer. Current and voltage outputs where measured with a Fluke 434 power quality analyzer. The Fluke measures currents and voltages in all 3 phases as well as the neutral, and give voltages, currents, power factor, and harmonics for each phase.

The initial plan was to run both the 10- and 14 pole machines at 400 rpm, to compare the machines under similar operation. The availability of the Fluke 434 changed this plan somewhat, as it is designed to operate from 40- to 70Hz, well below the electrical frequency of the 14 pole rotor at 400 rpm. The Fluke 434 can function at higher frequencies than 70Hz, but the harmonics calculation and frequency measurements give strange values if this is done.

B. Locked rotor testing

Locked rotor testing were performed to find the self and mutual inductances in much the same manner as for the FEM simulations. A signal generator where used to apply a current to one of the phases, while an oscilloscope where used to measure the current, as well as all the phase voltages. The measurements where done for all 3 phases for different 25 rotor positions through one full electrical rotation of the rotor. The mutual inductances could be calculated using Equation (7) as done in the FEM simulations, while the self inductance equation must be modified. The resistance in the winding give an angle between the current and voltage that is not 90^o. This is solved by including the angle of the current, giving Equation (11) and (10) for resistance and self inductance respectively. dq axis inductances can than be calculated from the self and mutual inductances by formula (12).

$$H_a = imag\left(\frac{v_{a\,Pk}\quad Pk}{i_{a\,Pk}\quad Pk \times e^{i\angle i_a} \times 2\pi f_e}\right) \tag{10}$$

$$R_a = real\left(\frac{v_{a\,Pk}\quad Pk}{i_{a\,Pk}\quad Pk \times e^{i\angle I_a}}\right) \tag{11}$$

$$\begin{bmatrix} L_0 & & \\ & L_d & \\ & & L_q \end{bmatrix} = W \begin{bmatrix} L_A & M_{AB} & M_{AC} \\ M_{BA} & L_B & M_{BC} \\ M_{CA} & M_{CB} & L_C \end{bmatrix} W^{\ 1} \tag{12}$$

The initial measurements gave very strange results with resistances up to 3 times the expected values as well as strange inductance results at certain rotor positions. The problem was mainly at lower frequencies such as 50-60Hz, disappearing at higher frequencies. The problems disappeared when the rotor where properly fastened, Figure (11), leading to the conclusion that mechanical resonance in the rotor can affect locked rotor measurements in a negative way if the rotor is insufficiently fastened, a strong elastic band where therefore used on the lever controlling the rotor position, to better lock the rotor into the desired position, this worked well on the 10 pole rotor, but vibrations where still present in the 14 pole setup.

VII. Results 10 pole rotor

A. Flux densities from FEM simulations

Figure (14) show the flux density of the 10 pole machine with the d axis lined up with phase a. Flux densities reach close to 3 Teslas in the pointy edges of the stator and rotor teeth, but generally co not exceed 2 Teslas except for the bridges connecting the stator segments together where an average of 2.5 Teslas are found.

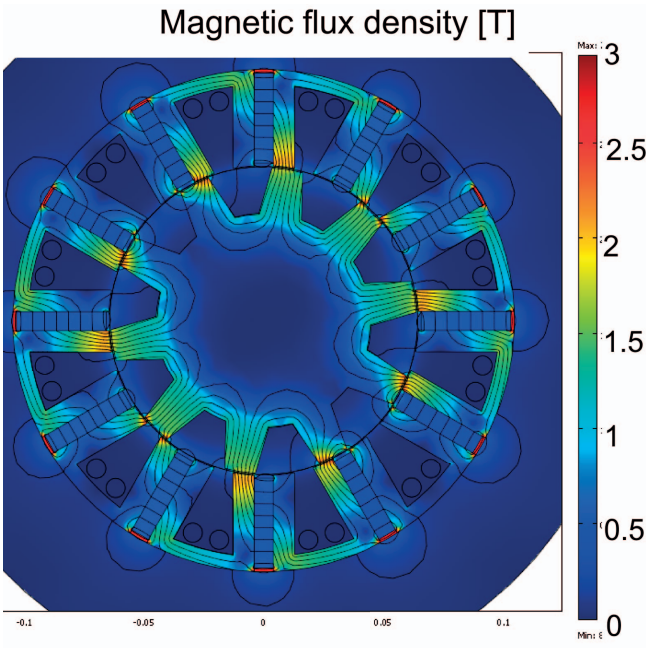

Figure 14. FEM plot of flux densities for 10-pole rotor

B. Back emf

The back emf waveforms from the 10 pole rotor no load test is seen Figure (15), with key characteristics listed in Table (III).

The average measured back emf is 11.3% lower than the FEM simulated value, this difference is expected since the simulation have been performed in 2-D, and corresponds with the ~10% difference between measurements and 2D simulations reported in [14].

Some voltage unbalance is present. with Vb being ~1.8% larger than Va. This is likely to be caused by the stator eccentricity and possibly other differences between the coils. It can be observed that the voltage of phase b appears to have a phase angle $\neq$120 degrees to the neighboring phases, this might also be caused by the stator eccentricity, or simply a measurement error. More detailed measurements of the air gap and the emf waveforms will be needed if this is to be examined further.

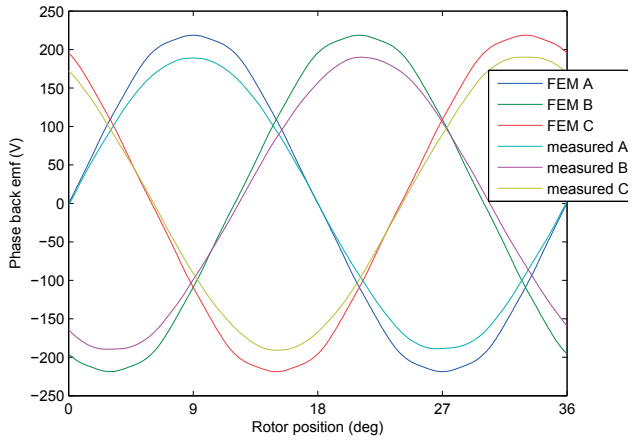

Figure 15. Comparison of FEM and measured results for 10 pole rotor at 67.7 Hz

Table III
KEY RESULTS FROM 10 POLE ROTOR AT 67.7 HZ

Parameter	FEM	Measured
Va peak	218.7	192.3
Vb peak	218.7	195.7
Vc peak	218.7	194.1
THD a	1.5%	1.2%
THD b	1.5%	1.3%
THD c	1.5%	1.4%

Individual stator pole back-emf: Figure (16) show the back

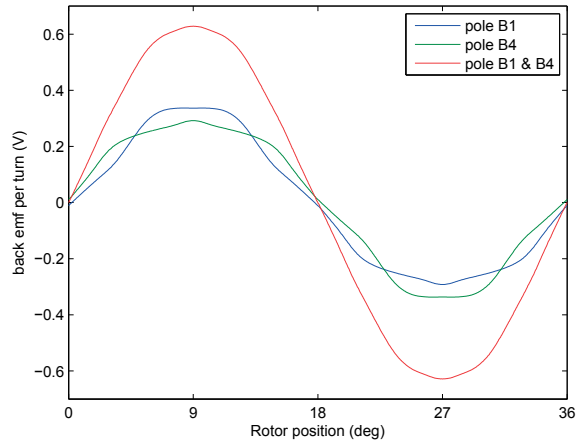

Figure 16. FEM simulations of induced voltages for pole B1 and B4, with 10 poled rotor at 67.7 Hz

emf waveform of the to different stator teeth in the 12/10 FSPM machine, as well as the smooth sinusoidal back emf that the combined waveforms give, this is well covered in [16]. The measurement results from Figure (17) coincides fairly well with the general waveform of the FEM results, but the back emf of pole (B1) is seen to be larger than that of pole (B4), this is natural as the eccentricity of the stator give an air gap of ~0.8mm at pole (B1) while pole (B4) have an air gap of ~1.2mm.

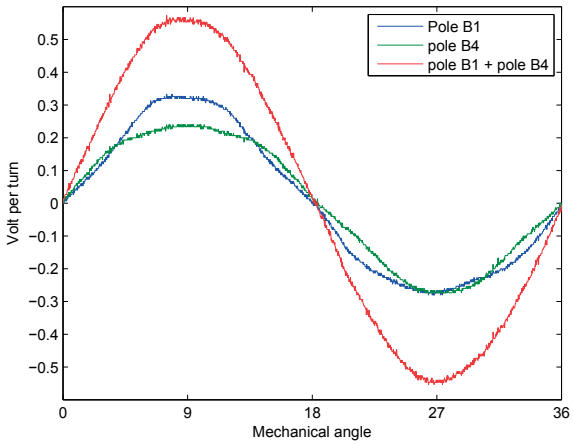

Figure 17. Measurements of induced voltages for pole B1 and B4, with 10 poled rotor at 67.7 Hz

C. Inductances from locked rotor test

The inductances as found in the FEM simulation and by locked rotor testing are shown in Figure (18), (19) and (20), and are listed in Appendix (IV and V). Both self and mutual inductance measurements are seen to be close to equal with the FEM values, but to vary less with position. The lowered position dependency is probably due to end effects that are neglected in the 2D simulations, and perhaps measurement inaccuracies.

Low ripple is seen i both the FEM- and measured results, and should give low ripple in the machine torque.

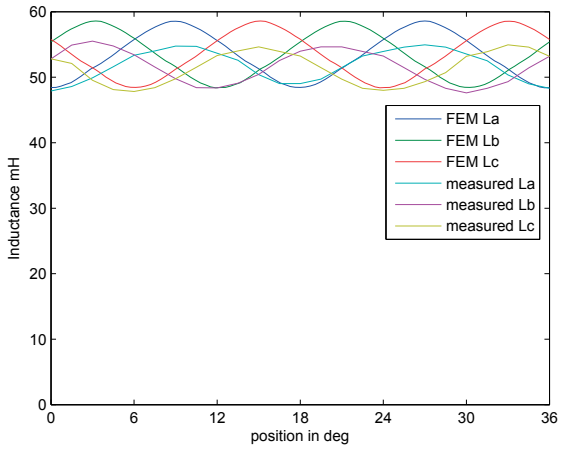

Figure 18. Self inductances for 10 pole rotor

D. Cogging

The cogging torque FEM simulation results for the round stator 10 pole machine is shown in Figure (21) , 6 identical cogging periods with a maximum torque of ~0.7Nm are observed, as expected from theory. Figure (22), shows how this changes dramatically if the simulation is conducted with an eccentric stator .

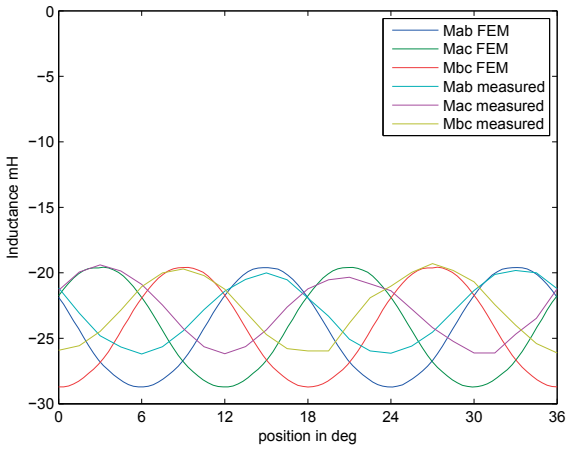

Figure 19. Mutual inductances for 10 pole rotor

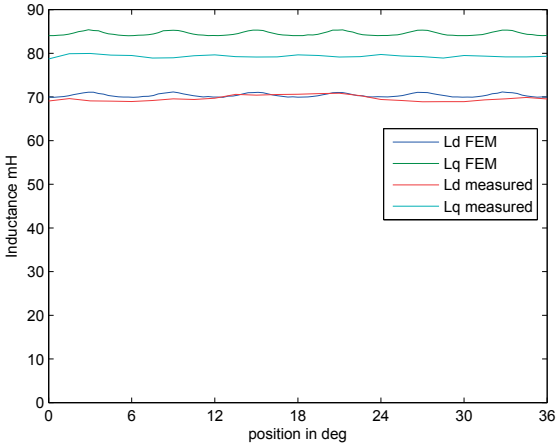

Figure 20. d- and q axis inductances for 10 pole rotor

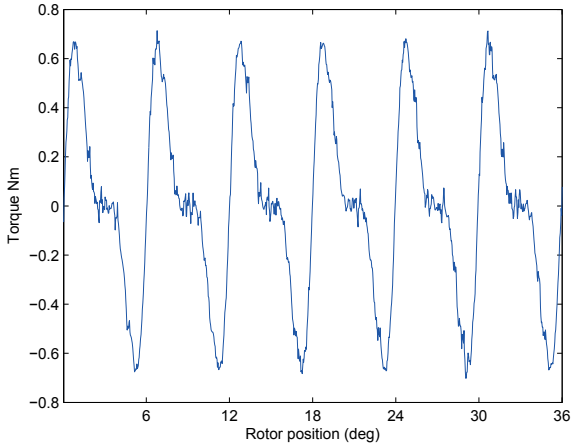

Figure 21. Cogging torque from round stator FEM simulation of 10 pole rotor

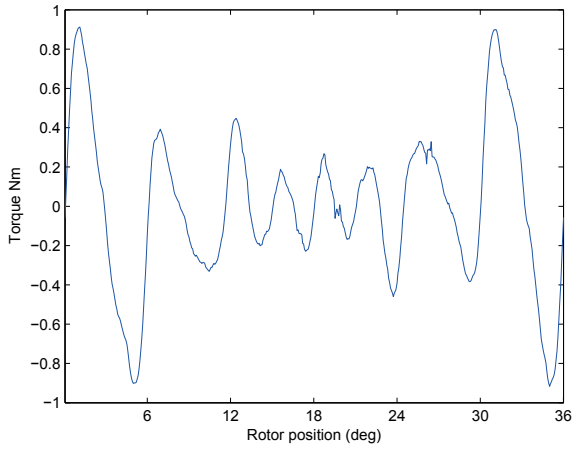

Figure 22. Cogging torque from eccentric stator FEM simulation of 10 pole rotor

Measurements where difficult to perform accurately, as the torque sensor only gave feedback of in a resolution of 0.1 Nm with a measurement uncertainty of 0.2 Nm. Some tests where still performed by turning the shaft on the motor side of the generator manually and reading off a peak torque cogging of $\pm$1.7Nm. The cogging torque have not been plotted as a function of position, but the tests confirmed that the machine cogging did not repeat with the pattern predicted for a round stator. This is ~5.7% of the maximum load torque found for the machine, but should improve well with a round stator.

E. Loaded machine performance

The machine was tested with a combination of resistive, capacitive loading, as well as short circuit testing, at both rated- and double speed. A summary is listed in Table (IV), with more information listed in Appendix (II).

Table IV
AVERAGE VALUES FOR 10 POLE MACHINE IN V, A AND W

Wye connected load	V_{rms}	I_{rms}	$cos(\phi)$	P_{el}	P_{shaft}	η
$no\,load\,400rpm$	136.3	0	_	-	33.5	-
$40\Omega\,400_{rpm}$	93.17	2.23	1	623	708	0.88
$40\Omega\|\|40\mu F\,400_{rpm}$	118	3.44	0.823	994	1167	0.85
$40\mu F\,400_{rpm}$	214.1	3.52	0	-	201	_
$80\|\|40\mu F\Omega\,400_{rpm}$	172.89	3.6	0.613	1129	1340	0.84
$shorted\,400_{rpm}$	_	3.24	_	-	117	_
$no\,load\,800rpm$	267.27	_	_	-	33.5	_
$80\Omega\,800_{rpm}$	182.8	2.33	1	1279	1407	0.91

The machine is seen to give an electrical power of $1129W$ with $cos(\phi) = 0.61$ at 400 rpm, this is a power density of $538kW/m^3$, which is quite satisfactory for a machine whose specifications certainly could have been optimized more, and whose power factor are decided by the available loads.

Torque density the machine run as a motor is perhaps just as interesting as the power density in generator mode. This in somewhat difficult to calculated from generator tests as the resistive losses in the machine will have to be added to the power output to find the power and hence torque in motoring mode of the machine. A simple way to calculate the motoring

torque is to assume that resistive losses are equal to total losses minus no load losses, theoretical motoring torque are than calculated from generator tests as shaft power minus no load torque. This give a theoretical motoring torque of 31.2 Nm for the $cos(\phi) = 0.61$ case, a torque density of 15.3 Nm/m^3.

Some attempts on calculation of $i_d$and $i_q$could of course have been done, but the results would end up as mostly guesswork as the inductances changes with loading, at least with current in the d axis, as this can be calculated from the short a short circuit test as by disregarding the winding resistance. The machine will than run with a power angle of ~90 degrees giving current along the negative d-axis, reducing the saturation in machine. $L_d = \frac{V_{no\,load}}{I_{short\,ciurcuit} \times 2\pi f_e} = 9.6H$, almost 40% more than the value form the locked rotor testing. A positive d-axis current should than give a decreased inductance, as this would increase saturation. An positional encoder would have given the power angle, and thereby the ability to find more detailed information about the machine inductances and performance.

F. Losses

Losses can generally be divided into friction and windage, iron losses and resistive losses. Friction, windage and iron losses are hard to separate in a PM machine, but are easily found collectively as the no load shaft power, 33.4- and 67 W in the 10 pole machine at 400 and 800 rpm respectively.

A loaded machine will additionally have current losses, $P = 3I^2R$. The resistances of the machine where measured with an RLC-meter before the rotor where mounted with results shown in Table (V). Measurements where performed with the rotor as well, but theory did not differ significantly except for the fact that they appeared to increase if the rotor where not locked tight into position. In examining the loaded machine performance it was found that the summation of no load losses and $P = 3I^2R$ gave close to the measured losses.

Table V
NO ROTOR RESISTANCE TESTS

frequency\pole	A	B	C
0Hz	2.98	2.99	3.00
60Hz	3.30	3.30	3.32
100Hz	3.51	3.51	3.53

VIII. RESULTS 14 POLE ROTOR

The test setup of the 14 pole rotor are equal to that of the 10 pole rotor with the exception that phase B and C have been changed to be able to use the same dq equations. The coil names for the examination of the individual stator teeth have however been kept the same.

A. Flux densities from FEM simulations

Figure (23) show the flux density of the 14 pole machine with the d axis lined up with phase a. The flux densities are generally close to the values of the 10 pole machine, flux densities reach close to 3 Teslas in the pointy edges, but generally co not exceed 2 Teslas except for the bridges connecting the stator segments. There are however more leakage flux than in the 10 pole machine.

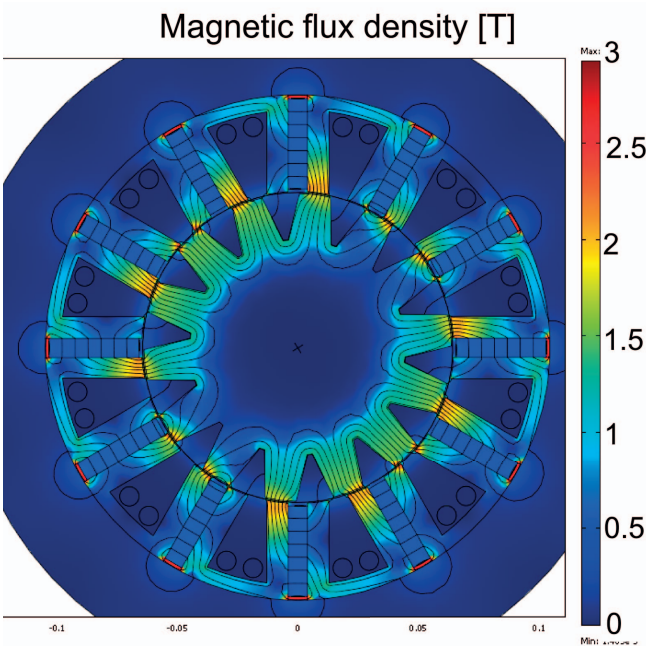

Figure 23. FEM plot of flux densities for 14-pole rotor

B. Back emf

Figure (24) shows the no load waveforms of the simulated and measured values of the 14 pole machine[2]. Table (VI) show the key characteristics compared to the FEM values. The measured voltages are ~11.5% lower than the simulated values a reasonable decrease when end effects are considered. The back emf increases almost 10% over the 10 pole machine, promising a similar increase in torque (Equation (5)) at the same i_q, provided the back emf are independent of the load current.

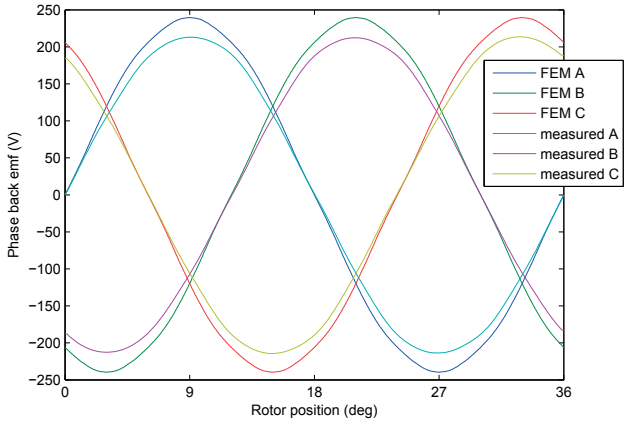

Figure 24. Comparison of FEM and measured results for 14 pole rotor at 400rpm/94.9 Hz

Individual stator pole back-emf: Figure (26) and (25) show the simulated and measured values for the back emf through coil B1 and B4 as well as the sum of the two. There are

[2]The measurements for the plot have been taken at 67.9 Hz, and scaled up 1.4 times to a 400 rpm (94.88 Hz) due to measurement conveniences

Table VI
KEY RESULTS FROM 14 POLE ROTOR AT 94.9 HZ

Parameter	FEM	Measured
Va peak	239.5	212.2
Vb peak	239.5	210.9
Vc peak	239.5	212.8
THD a	1.1%	1.1%
THD b	1.1%	0.9%
THD c	1.1%	1.1%

apparently less difference between the back emf of coils here than the case is for the 10 pole machine, the effect of this difference on machine performance would be interesting to examine more closely. The back emf of the B1 measurements is seen to be larger than that of B4 just as the case was with the 10 pole machine, as expected from the air gap differences.

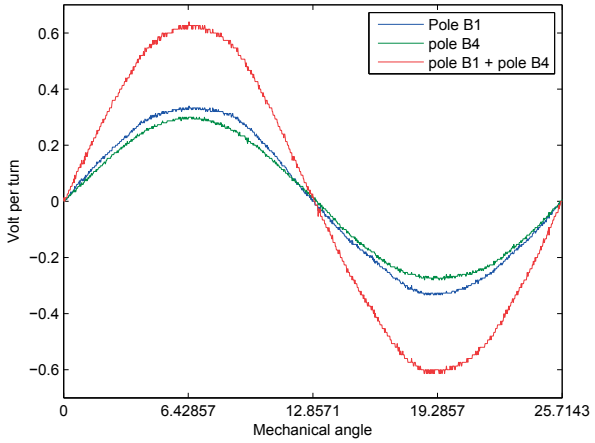

Figure 25. Measurements of induced voltages for pole B1 and B4, with 14 poled rotor at 400 rpm

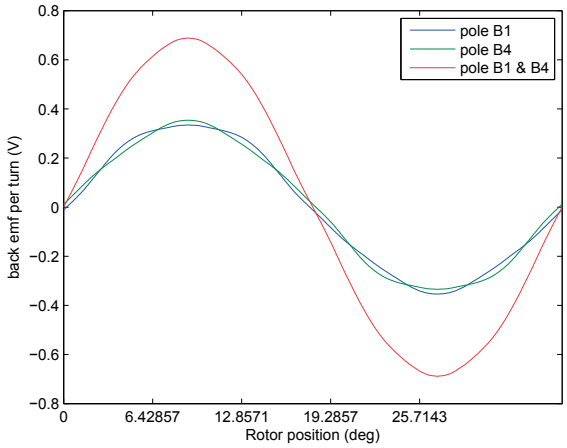

Figure 26. FEM simulation of induced voltages for pole B1 and B4, with 14 poled rotor at 400 rpm

C. Inductances from locked rotor test

Figure (27) (28) and (29), with numbers listed in Appendix (VI and VII), show the self-, mutual- and dq inductances from the locked rotor testing of the machine. The measurements coincide very well at first, but are seen to get weary strange as the rotor angle increases. This have been identified as a current clamp that gradually ran out of battery giving lower and lower current measurements and hence higher inductance values are calculated, there where not time to repeat the measurements, but the first part of the measurements are assumed to be correct and representative for the machine.

The inductances are seen ~15% larger than those of the 10 pole machine, as should be expected with more steel in the rotor. A much more important difference between the 10 and 14 pole machine is that f_e/rpm and thereby the reactance per inductance is effectively 40% higher in the than in the 10 pole machine. This is factor is important in the dimensioning of possible frequency drives and for the possibility of driving the machine in field weakening mode.

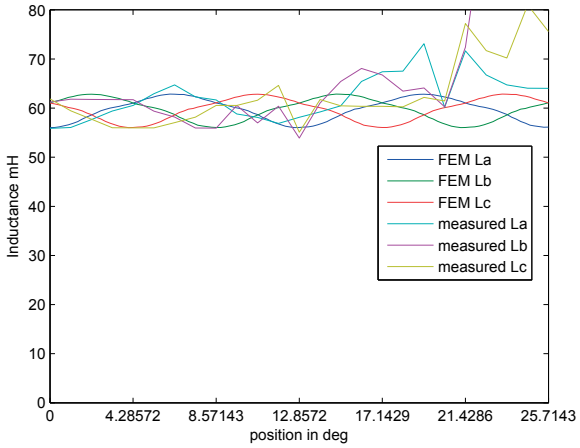

Figure 27. Self inductances for 14 pole rotor

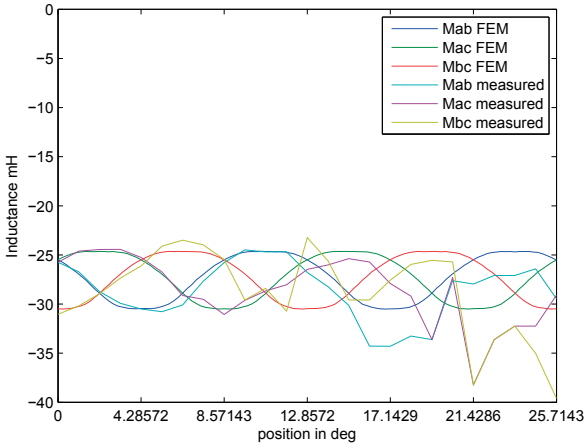

Figure 28. Mutual inductances for 14 pole rotor

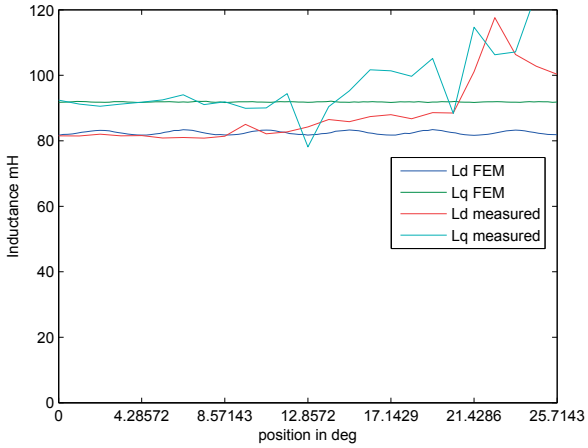

Figure 29. d- and q axis inductances for 14 pole rotor

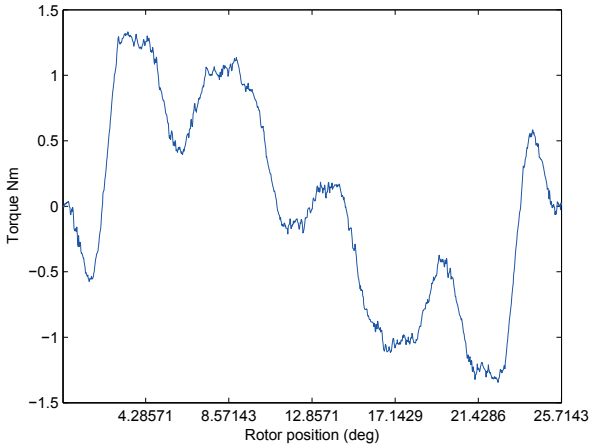

Figure 31. Cogging torque from FEM simulation with 14 pole rotor and eccentric stator

D. Cogging

The cogging torque found in FEM simulation of the 14 pole machine, with round and eccentric stator, are shown in Figures (30) and (31). The simulation promises low cogging with a round stator, while the stator eccentricity are shown to have a very adverse effect.

Simple measurements give a cogging of max ± 1.6 Nm varying with a pattern related to the simulation of the eccentric stator, this is ~5.5% of the maximum electrical torque achieved, but should be improved much with a round stator..

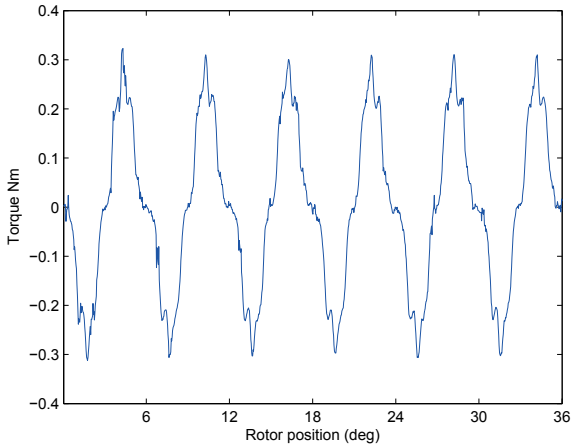

Figure 30. Cogging torque from FEM simulation with 14 pole rotor and round stator

E. Loaded machine performance

Some of the measurements done for the 14 pole machine is shown in Table (VII) with a more extensive set shown in Appendix(III).

The machine give $1147W$ at $cos(\phi) = 0.6$ a power density of $546kW/m^3$. A little better than the 10 pole machine, at a lower current loading and lower power factor, but at higher voltage. The torque density in a theoretical motoring mode can be calculated just as done for the 10 pole rotor in (VII-E), this will for the generator case just examines give a torque density of 15.3 Nm/m^3f, just as for the 10 pole machine, but the current is lower, and with the correct frequency drive it should be possible to get more torque from the 14 pole machine than the 10 poled.

Further comparison is difficult, as the power angle is unknown, and thereby also the i_d and i_q.

The 14 pole machine suffers from saturation just as the 10 pole, the short circuit test give $L_d = \frac{V_{no\,load}}{I_{short\,ciurcuit} \times 2\pi f_e} = 10.6H$, almost 30% higher than the locked rotor test. The difference is not as large as for the 10 pole machine, but the current is also lower.

Table VII
AVERAGE PHASE VALUES FOR 14 POLE MACHINE IN V, A AND W

Wye connected load	V_{rms}	I_{rms}	$cos(\phi)$	P_{el}	P_{shaft}	η
$no\,load\,400_{rpm}$	149.7	-	-	-	33.5	-
$40\Omega\,400_{rpm}$	80.7	1.9	1	467	540	0.86
$40\Omega \| \| 40\mu F\,291_{rpm}$	88.7	2.6	0.82	550	683	0.83
$40\mu F\,291_{rpm}$	207	3.59	0	-	180	-
$80\Omega \| \| 40\mu F\,291_{rpm}$	145.2	3.1	0.6	796	951	0.84
$32\Omega_{series} 40\mu F\,400_{rpm}$	186	3.4	0.6	1147	1340	0.86
$shorted\,400_{rpm}$	-	2.35	-	-	83.8	-
$no\,load\,800_{rpm}$	298.4	-	-	-	84	-
$160\Omega\,800_{rpm}$	234	1.43	1	1005	1123	0.89

F. Losses

The 14 pole machine have no load losses of 33.4- and 84 W at 400- and 800 rpm respectively. This is the same as the 10 pole at 400 rpm, but more at 800 rpm. Iron losses are frequency dependent, and increases faster at higher frequencies, and the results show how the higher fundamental frequency of the 14 pole rotor is more important at higher rpms. The losses are likely to have increased at 400 rpms as well, but the coarse torque measurements at a 0.1Nm resolution and probably changed windage makes this hard to measure.

Resistance values from no rotor measurements are of course the same as for the 10 pole rotor, shown in Table (V). Measurements where performed with the rotor mounted, giving similar values as the no rotor case, but these where just as for the 10 pole very dependent on how the rotor where locked into place. The summation of no load losses and $P = 3I^2R$ gave close to the measured losses for the 14 pole machine, just as for the 10 pole, but this field needs to be examined more closely.

IX. FURTHER WORK

The machine should be tested with a frequency converter and a positional encoder. This would give the opportunity to run a pure q-axis current, giving a much better platform for an evaluation of the machine performance, both in terms of torque density and in examining the saturation issues present in the machine. A frequency converter would of course give the opportunity to run the machine as a motor as well as a generator.

Further work should also be put into the examination of losses and resistances, with more detailed measurements of the torque, to get better values for both the generator input power and hence the losses, and the cogging torque.

The stator eccentricity show little effect on the phase voltages, but some work should still be put into the examination of possible power fluctuation caused by this.

Still another task that can be performed are the testing of alternative rotors, such as skewing the rotors already made and testing of a more optimized 14 pole rotor

X. CONCLUSION

The FSPM machine concept have been studied, and a FSPM machine with a 12 pole stator and an interchangeable rotor of 10 and 14 poles have been built. The machine have been tested as a generator, with various resistive and capacitive loads, while locked rotor tests have been performed to plot the machine inductances as a function of rotor position, giving results close to the values found by FEM analysis. Both rotor configurations run smoothly with THD of less than 1.4% in no load and little more while loaded.

The 10- and 14 pole rotor have a measured 400 rpm phase back emf, of 136.3V and 149.7V rms respectively, giving the 14 pole a torque constant approximately 10% higher than that of the 10 pole. The load tests of both machines show a peak electrical power at 400rpm of ~1150W with a power density of ~540kW/m^3 at η~85%. The 14 pole rotor seems to be better than the 10 pole rotor, but comparison of the loaded machine performance is difficult without better control the the d- and q axis currents, especially as saturation issues causes the machine inductances to vary much with machine loading.

The machine stator where made with a slight eccentricity causing the air gap to vary from 0.8mm to 1.2mm, This is believed to have increased cogging, but does not seem to have effected the machine phase- voltages and currents much, as these keep within 2-3% each other at the tested loads.

ACKNOWLEDGMENTS

I would like to thank my supervisor Robert Nilssen for the opportunity to design and build a my own electric machine, Anyuan Chen for always taking time to answer my questions and Oddvar Landrø at the workshop, for great help with the practical building of the machine.

REFERENCES

[1] W. Hua, M. Cheng, H. Jia, and X. Fu, "Comparative Study of Flux-Switching and Doubly-Salient PM Machines Particularly on Torque Capability," in *IEEE Industry Applications Society Annual Meeting, 2008. IAS'08*, 2008, pp. 1–8.

[2] C. Wang, S. Nasar, and I. Boldea, "Three-phase flux reversal machine (FRM)," *IEE Proceedings-Electric Power Applications*, vol. 146, p. 139, 1999.

[3] S. Rauch, L. Johnson, N. AIEE, and C. Santa Barbara, ""Design principles of flux-switch alternators"," *Power Apparatus and Systems, Part III. Transactions of the American Institute of Electrical Engineers*, vol. 74, no. 3 Part III, pp. 1261–1268, 1955.

[4] E. Hoang, A. Ben Ahmed, and J. Lucidarme, "Switching flux permanent magnet polyphased synchronous machines," in *EUROPEAN CONFERENCE ON POWER ELECTRONICS AND APPLICATIONS*, vol. 3. PROCEEDINGS PUBLISHED BY VARIOUS PUBLISHERS, 1997, pp. 3–3.

[5] J. Chen, Z. Zhu, and D. Howe, "Stator and Rotor Pole Combinations for Multi-Tooth Flux-Switching Permanent-Magnet Brushless AC Machines," *IEEE Transactions on Magnetics*, vol. 44, no. 12, pp. 4659–4667, 2008.

[6] Z. Zhu, J. Chen, Y. Pang, D. Howe, S. Iwasaki, and R. Deodhar, "Analysis of a Novel Multi-Tooth Flux-Switching PM Brushless AC Machine for High Torque Direct-Drive Applications," *IEEE Transactions on Magnetics*, vol. 44, no. 11 Part 2, pp. 4313–4316, 2008.

[7] "Parallel path magnetic technology for high efficiency power generators and motor drives," http://www.flynnresearch.net/technology/PPMT technology white paper.pdf.

[8] J. Wang, W. Wang, K. Atallah, and D. Howe, "Design Considerations for Tubular Flux-Switching Permanent Magnet Machines," *IEEE Transactions on Magnetics*, vol. 44, no. 11 Part 2, pp. 4026–4032, 2008.

[9] H. Pollock, C. Pollock, R. Walter, and B. Gorti, "Low cost, high power density, flux switching machines and drives for power tools," in *Industry Applications Conference, 2003. 38th IAS Annual Meeting. Conference Record of the*, vol. 3, 2003.

[10] A. Thomas, Z. Zhu, G. Jewell, and D. Howe, "Flux-switching PM brushless machines with alternative stator and rotor pole combinations," in *Electrical Machines and Systems, 2008. ICEMS 2008. International Conference on*, 2008, pp. 2986–2991.

[11] W. Fei and J. Shen, "Comparative Study and Optimal Design of PM Switching Flux Motors," in *Universities Power Engineering Conference, 2006. UPEC'06. Proceedings of the 41st International*, vol. 2, 2006.

[12] J. Chen, Z. Zhu, A. Thomas, and D. Howe, "Optimal combination of stator and rotor pole numbers in flux-switching PM brushless AC machines," in *Electrical Machines and Systems, 2008. ICEMS 2008. International Conference on*, 2008, pp. 2905–2910.

[13] W. Fei and J. Shen, "Comparative study and optimal design of pm switching flux motors," vol. 2, Sept. 2006, pp. 695–699.

[14] Z. Zhu, Y. Pang, D. Howe, S. Iwasaki, R. Deodhar, and A. Pride, "Analysis of electromagnetic performance of flux-switching permanent-magnet machines by nonlinear adaptive lumped parameter magnetic circuit model," *IEEE Transactions on magnetics*, vol. 41, no. 11, pp. 4277–4287, 2005.

[15] Z. Zhu, Y. Pang, J. Chen, Z. Xia, and D. Howe, "Influence of design parameters on output torque of flux-switching permanent magnet machines," in *IEEE Vehicle Power and Propulsion Conference, 2008. VPPC'08*, 2008, pp. 1–6.

[16] W. Hua, M. Cheng, Z. Zhu, and D. Howe, "Analysis and Optimization of Back-EMF Waveform of a Novel Flux-Switching Permanent Magnet Motor," in *IEEE International Electric Machines & Drives Conference, 2007. IEMDC'07*, vol. 2, 2007.

Appendix I
Lumped parameter model

```
%Function modeling FSPM machines of any rotor/stator tooth combination by the
%use of air gap permeances.
%The machines are modelled with infinitely permeable stator- and rotor steel
%while air gap permeances are modelled withour any fringing effects.

%s_teeth=12;              %number of stator poles
%s_scaling=1.0;           %scaling factor of stator teeth vs base tooth width
%
%r_teeth=10;              %number of rotor teeth
%r_scaling=1.4;           %scaling factor of rotor teeth vs base tooth width
%
%base=15e-3;              %base tooth with (width of rotor and stator teeth,
magnets and winding slots)
%m_length=2;              %machine length in #base
%airgap=1e-3;             %air gap length
%magnet_length=base*3;    %length of magnets radially
%Br=1.2;                  %magnent remanance flux


%tann                     %avreage flux density in stator tooth number one
%coil                     %coil(#,x)= flux in tooth # for step number x;

function [coil tann] = fluxs2...
(s_teeth,r_teeth,s_scaling,r_scaling,airgap,base,m_length,magnet_length,Br)

my_0=4*pi*1e-7; %my0



Am=(magnet_length)*(base*m_length);%magnet area
lm=base*(2-s_scaling); %magnet length
Ym=my_0*Am/lm; %magnet permeability

phi_r=Br*Am;

stator=0:base*2:base*(4*(s_teeth)-1);   %middle of stator teeth


O=base*4*s_teeth;
base_rotor=-O/r_teeth:O/r_teeth:O/r_teeth*r_teeth;     %middle if rotor teeth




min_slot=min(base*[r_scaling s_scaling]); %the smallest tooth width



step=0;
```

```
for displasement=0:0.02*base:0/r_teeth-0.02*base %moving the rotor
step=step+1;

    rotor=base_rotor+displasement;
    i=0;
    Y=inf(1,length(stator));
    for s_tooth=stator
        i=i+1;
        gap_w=0;
        for r_tooth=rotor   %calculation of stator/rotor air gap width for use
in reluctance calculations
            tmp=abs(s_tooth-r_tooth)-base*abs(r_scaling-s_scaling)/2;
            if tmp<0
                gap_w=min_slot;
            elseif tmp<min_slot
                gap_w=min_slot-tmp;
            end
        end
        R_air=airgap/(gap_w*base*m_length*my_0);
        Y(i)=1/R_air; %admittance of different stator/rotor air gaps

    end

    %setting up Y matrix
    for counter=2:(length(Y)/2-1)
        Ymat(counter,counter)=Y(2*counter-1)+Y(2*counter)+2*Ym;
        Ymat(counter,counter+1)=-Ym;
        Ymat(counter,counter-1)=-Ym;
    end
    Ymat(1,1)=Y(2*1-1)+Y(2*1)+2*Ym;
    Ymat(1,1+1)=-Ym;
    Ymat(length(Y)/2,length(Y)/2)=Y(length(Y)-1)+Y(length(Y))+2*Ym;
    Ymat(length(Y)/2,length(Y)/2-1)=-Ym;
    Ymat(1,length(Y)/2)=-Ym;
    Ymat(length(Y)/2,1)=-Ym;


%setting up magnet flux sources
for counter=1:length(Ymat)
    phi(counter,1)=-(-1)^counter*2*phi_r;
end

%solving the matix equations equations:
Um=inv(Ymat)*phi; %Um=magnetisk potensiale;


for i=1:length(Ymat)-1    %calculating coil flux linkeages
coil(i,step)=Um(i)*Y(i*2)+Um(i+1)*Y(i*2+1);
end
coil(length(Ymat),step)=Um(length(Ymat))*Y(length(Ymat)*2)+Y(1)*Um(1);
tann(step)=Um(1)*Y(1)/(base^2*m_length*s_scaling); % avreage flux density in
stator tooth number one
end
```

Appendix II

Measurements results on tests done with the 10 poled rotor

(El torque is a help value for comparing different rotor speeds defiened as power output, W, divided by shaft speed (rad/s))

40 ohm 40uF in parallell — **400 rpm**

	A	B	C	Avg	Total	
V	117,700	117,740	118,660	118,0333	0	
I	3,46	3,39	3,47	3,44	0	
Cos(phi)	,820	,820	,830	0,823333	0	
VA	407,2	399,2	411,7334	406,0445	1218,1334	
W	331,4666	325,0666	337,6	331,4667	994,4	
Var	236,5334	231,4666	235,7334	234,4889	703,4666	
Shaft power					1168,67247	W
Shaft torque					27,9	Nm
El torque					23,7395513	Nm
Efficiency					0,85087998	

40uF — **400 rpm**

	A	B	C	Avg	Total	
V	215,3	213,61	213,53	214,1467	0	
I	3,598	3,452	3,534	3,528	0	
Cos(phi)	0	0	0	0	0	
VA	774,4	737,3334	754,6666	755,5556	2266,667	
W	-6,4	-6,9334	-9,0666	-7,555533	-22,6666	
Var	774,4	737,3334	754,6666	755,4667	2266,4	
Shaft power					201,0619	W
Shaft torque					4,8	Nm
El torque					-0,541125	Nm
Efficiency					-0,112734	

No load — **400 rpm**

	A	B	C	Avg	Total	
V	135,87	136,83	136,2	136,3	0	
I	0,002	0,002	0,004	0,002667	0	
Cos(phi)	0,01	0,01	0,01	0,01	0	
VA	0,2666	0,2666	0,5334	0,444467	1,3334	
W	0	0	0	0	0	
Var	0,2666	0,2666	0,5334	0,355533	1,0666	
Shaft power					33,5103216	W
Shaft torque					0,8	Nm
El torque					0	Nm
Efficiency					0	

80 ohm 40uF in parallell — **400 rpm**

	A	B	C	Avg	Total	
V	173,59	172,11	172,97	172,89	0	
I	3,664	3,55	3,624	3,612667	0	
Cos(phi)	0,61	0,61	0,62	0,613333	0	
VA	636	610,9334	626,9334	624,7111	1874,133	
W	381,3334	367,7334	380,5334	376,4445	1129,333	
Var	509,3334	487,7334	498,4	498,4889	1495,467	
Shaft power					1340,413	W
Shaft torque					32	Nm
El torque					26,96085	Nm
Efficiency					0,842527	

40 ohm — **400 rpm**

	A	B	C	Avg	Total	
V	92,63	93,61	93,28	93,17333	0	
I	2,23	2,206	2,256	2,230667	0	
Cos(phi)	1,01	1,01	1,01	1,01	0	
VA	206,6666	206,4	210,4	207,8222	623,4666	
W	206,6666	206,4	210,4	207,8222	623,4666	
Var	3,4666	5,6	1,8666	3,644467	10,9334	
Shaft power					707,905545	W
Shaft torque					16,9	Nm
El torque					14,8841687	Nm
Efficiency					0,88072004	

no load — **800 rpm**

	A	B	C	Avg	Total	
V	266,41	268,34	267,05	267,2667	0	
I	0,002	0,004	0,004	0,003333	0	
Cos(phi)	0,01	0,01	0,01	0,01	0	
VA	0,5334	0,8	1,3334	0,888867	2,6666	
W	0	0	0	0	0	
Var	0,2666	0,2666	0,5334	0,266667	0,8	
Shaft power					67,02064	W
Shaft torque					0,8	Nm
El torque					0	Nm
Efficiency					0	

Short circuit — **400 rpm**

	A	B	C	Avg	Total	
V	0,62	1,19	0,63	0,813333	0	
I	3,24	3,21	3,278	3,242667	0	
Cos(phi)	0,01	0,76	0,01	0,26	0	
VA	2,1334	3,7334	2,1334	2,755533	8,2666	
W	0	0,2666	0,2666	0,1778	0,5334	
Var	2,1334	3,7334	-2,1334	1,244467	3,7334	
Shaft power					117,286126	W
Shaft torque					2,8	Nm
El torque					0,01273399	Nm
Efficiency					0,00454785	

80 ohm — **800 rpm**

	A	B	C	Avg	Total	
V	181,65	183,86	182,76	182,7567	0	
I	2,33	2,308	2,36	2,332667	0	
Cos(phi)	1,01	1,01	1,01	1,01	0	
VA	423,2	424,2666	431,4666	426,3111	1278,933	
W	423,2	424,2666	431,4666	426,2222	1278,667	
Var	-1,8666	3,7334	-2,9334	-0,355533	-1,0666	
Shaft power					1407,434	W
Shaft torque					16,8	Nm
El torque					15,26296	Nm
Efficiency					0,908509	

Appendix III

Measurements results on tests done with the 14 poled rotor

(El torque is help value for comparing different rotor speeds, defiened as power output, W, divided by shaft speed (rad/s))

no load — **291 rpm**

	A	B	C	Avg	Total
V	0 A	B	C	Avg	
I	V	109,32	108,52	109,12	108,9866667
Cos(phi)	I	0,002	0,004	0,006	0,004
VA	Cos(phi)	0,01	0,01	0,01	0,01
W	kVA	0,2666	0,5334	0,5334	0,444466667
Var	KW	0	0	0	0
Shaft power					24,37875899
Shaft torque					0,8
El torque					0,014585375
Efficiency					0,018231718

40 ohm 40uH in paralell — **291 rpm**

	A	B	C	Avg	Total
V	88,9	87,75	89,41	88,68667	0
I	2,628	2,528	2,632	2,596	0
Cos(phi)	0,82	0,82	0,82	0,82	0
VA	233,6	221,8666	235,2	230,3111	690,9334
W	189,0666	179,7334	191,4666	186,7555	560,2666
Var	137,0666	129,8666	136,8	134,6667	404
Shaft power					667,3685
Shaft torque					21,9
El torque					18,3854
Efficiency					0,839516

40 ohm — **400 rpm**

	A	B	C	Avg	Total
V	80,750	80,490	80,920	80,72	0
I	1,944	1,884	1,958	1,928667	0
Cos(phi)	1,010	1,010	1,010	1,01	0
VA	157,0666	151,4666	158,4	155,6445	466,9334
W	157,0666	151,4666	158,4	155,6445	466,9334
Var	1,3334	1,3334	1,0666	1,244467	3,7334
Shaft power					540,3539364
Shaft torque					12,9
El torque					11,14721381
Efficiency					0,864125101

no load — **400 rpm**

	A	B	C	Avg	Total
V	150,12	149,06	149,88	149,6867	0
I	0,002	0,004	0,004	0,003333	0
Cos(phi)	0,01	0,01	0,01	0,01	0
VA	0,2666	0,5334	0,8	0,533333	1,6
W	0	0	0	0	0
Var	0	0,2666	0,2666	0,1778	0,5334
Shaft power					33,51032
Shaft torque					0,8
El torque					0
Efficiency					0

oscillating machine giving bad readouts:

40 ohm 40uH in parallell — **400 +-2 rpm**

	A	B	C	Avg	Total
V	87,45	88,44	86,74	87,54333	0
I	2,938	2,88	2,922	2,913333	0
Cos(phi)	0,66	0,78	0,74	0,726667	0
VA	256,8	254,6666	253,6	255,0222	765,0666
W	184	181,3334	184,5334	183,2	549,6
Var	179,2	178,9334	173,8666	177,4222	532,2666
Shaft power					682,7728034
Shaft torque					16.3+-0.2Nm
El torque					13,12073351
Efficiency					0,804952976

80 ohm — **400 rpm**

	A	B	C	Avg	Total
V	114,54	114,54	113,85	114,31	0
I	1,464	1,43	1,462	1,452	0
Cos(phi)	1,01	1,01	1,01	1,01	0
VA	167,7334	164	166,4	166,0445	498,1334
W	167,7334	164	166,4	166,0445	498,1334
Var	1,3334	2,1334	1,0666	1,6	4,8
Shaft power					557,1091
Shaft torque					13,3
El torque					11,89206
Efficiency					0,89414

40uH — **291 rpm**

	A	B	C	Avg	Total
V	209,41	205,1	206,52	207,01	0
I	3,584	3,384	3,488	3,485333	0
Cos(phi)	0	0	0	0	0
VA	750,6666	693,8666	720,5334	721,7778	2165,3334
W	-4,2666	-4,5334	-9,3334	-6,04447	-18,1334
Var	750,6666	693,8666	720,2666	721,6	2164,8
Shaft power					179,7933476
Shaft torque					5,9
El torque					-0,59505572
Efficiency					-0,1008569

Short circuit — **400 rpm**

	A	B	C	Avg	Total
V	0,27	0,26	0,15	0,226667	0
I	2,362	2,312	2,376	2,35	0
Cos(phi)	0,01	0,01	0,01	0,01	0
VA	0,5334	0,5334	0,2666	0,533333	1,6
W	0,5334	0,2666	-0,2666	0,1778	0,5334
Var	0,5334	-0,5334	0,2666	0,088867	0,2666
Shaft power					83,7758
Shaft torque					2
El torque					0,012734
Efficiency					0,006367

80 ohm — **800 rpm**

	A	B	C	Avg	Total
V	156,12	155,82	156,14	156,0267	0
I	2	1,946	2,014	1,986667	0
Cos(phi)	0,01	0,01	0,01	0,01	0
VA	312,2666	303,4666	314,4	310,0445	930,1334
W	312,2666	303,4666	314,4	309,9555	929,8666
Var	-2,9334	-1,0666	-3,7334	-2,48887	-7,4666
Shaft power					1063,952712
Shaft torque					12,7
El torque					11,09946494
Efficiency					0,873973617

Short cicuit — **291 rpm**

	A	B	C	Avg	Total
V	0,22	0,21	0,11	0,18	0
I	2,36	2,308	2,374	2,347333	0
Cos(phi)	0,01	0,01	0,01	0,01	0
VA	0,5334	0,5334	0,2666	0,444467	1,3334
W	0,5334	0,2666	0	0,1778	0,5334
Var	0,2666	-0,2666	0,2666	0,088867	0,2666
Shaft power					73,13628
Shaft torque					2,4
El torque					0,017504
Efficiency					0,007293

No load — **800 rpm**

	A	B	C	Avg	Total
V	299,24	297,16	298,82	298,4067	0
I	0,002	0,004	0,008	0,004667	0
Cos(phi)	0,01	0,01	0,01	0,01	0
VA	0,2666	1,0666	2,1334	1,333333	4
W	0	0	0	0,088867	0,2666
Var	0,2666	0,2666	0,8	0,444467	1,3334
Shaft power					83,7758041
Shaft torque					1
El torque					0,003182303
Efficiency					0,003182303

160 ohm — **800 rpm**

	A	B	C	Avg	Total
V	236,92	232,8	232,26	233,9933	0
I	1,434	1,42	1,44	1,431333	0
Cos(phi)	0,01	0,01	0,01	0,01	0
VA	339,7334	330,6666	334,4	334,9333	1004,8
W	339,7334	330,6666	334,1334	334,8445	1004,533
Var	1,0666	1,0666	-10,1334	-2,66667	-8
Shaft power					1122,596
Shaft torque					13,4
El torque					11,99073
Efficiency					0,894831

80 ohm 40uH in paralell			**291 rpm**		
	A	B	C	Avg	Total
V	146,48	143	146,22	145,2333	0
I	3,134	2,976	3,1	3,07	0
Cos(phi)	0,6	0,61	0,61	0,606667	0
VA	458,9334	425,6	453,0666	445,8667	1337,6
W	272,2666	253,3334	270,6666	265,3333	796
Var	369,3334	342,1334	363,4666	358,2222	1074,6666
Shaft power					950,7716007
Shaft torque					31,2
El torque					26,12109994
Efficiency					0,837214742

32 ohm 40uH in series			**400 rpm**		
	A	B	C	Avg	Total
V	184,6	185,69	188,02	186,1033	0
I	3,398	3,328	3,468	3,398	0
Cos(phi)	0,6	0,6	0,59	0,596667	0
VA	627,4666	617,8666	652	632,5333	1897,6
W	382,9334	372,2666	392,5334	382,5778	1147,733
Var	496,8	493,0666	520,8	503,5555	1510,667
Shaft power					1340,413
Shaft torque					32
El torque					27,40012
Efficiency					0,856254

40 ohm 40uH in series			**400 rpm**		
	A	B	C	Avg	Total
V	174,15	174,43	177,06	175,2133	0
I	2,914	2,836	2,962	2,904	0
Cos(phi)	0,69	0,68	0,68	0,683333	0
VA	507,2	494,6666	524,2666	508,8	1526,4
W	352,5334	340,8	360,2666	351,1111	1053,3334
Var	364,8	358,4	381,0666	368,1778	1104,5334
Shaft power					1202,182789
Shaft torque					28,7
El torque					25,1464826
Efficiency					0,876184063

80 ohm 40uH in series			**400 rpm**		
	A	B	C	Avg	Total
V	156,22	155,74	157,07	156,3433	0
I	1,752	1,704	1,768	1,741333	0
Cos(phi)	0,88	0,87	0,87	0,873333	0
VA	273,6	265,3334	277,8666	272,2667	816,8
W	239,2	230,6666	241,8666	237,2445	711,7334
Var	132,8	131,2	136,5334	133,6	400,8
Shaft power					791,6813
Shaft torque					18,9
El torque					16,99138
Efficiency					0,899015

Appendix IV

Inductance values fom FEM calculation for the 10 poled rotor, in Henries

Angle	La	Lb	Lc	Lab	Lac	Lbc	Ld	Lq
0	0,048423	0,055404	0,055761	-0,02188	-0,02175	-0,02871	0,070003	0,084069
1,08	0,04892	0,05691	0,054148	-0,02368	-0,0204	-0,02848	0,070111	0,084206
2,16	0,050139	0,058049	0,052473	-0,02555	-0,01968	-0,02768	0,070744	0,084971
3,24	0,051662	0,058585	0,051124	-0,02708	-0,01957	-0,02654	0,071098	0,085228
4,32	0,053142	0,057966	0,049572	-0,02807	-0,01997	-0,02478	0,070337	0,084467
5,4	0,054846	0,056776	0,048574	-0,02866	-0,02105	-0,02286	0,069971	0,084088
6,48	0,056404	0,055248	0,048509	-0,02866	-0,0226	-0,02126	0,069996	0,084147
7,56	0,05771	0,053571	0,049236	-0,0281	-0,0245	-0,0201	0,070346	0,084449
8,64	0,058529	0,052081	0,050678	-0,02713	-0,02631	-0,01962	0,070998	0,085216
9,72	0,05828	0,050537	0,052174	-0,02561	-0,02757	-0,01966	0,070716	0,085002
10,8	0,057249	0,04912	0,053703	-0,02373	-0,0284	-0,02025	0,070162	0,084227
11,88	0,055761	0,048388	0,055404	-0,02191	-0,02871	-0,02154	0,069977	0,084072
12,96	0,054148	0,048638	0,05691	-0,02053	-0,02848	-0,02323	0,070179	0,084195
14,04	0,052473	0,049634	0,058049	-0,01972	-0,02768	-0,02513	0,070724	0,084832
15,12	0,051124	0,051267	0,058585	-0,01961	-0,02654	-0,0268	0,071073	0,085305
16,2	0,049572	0,05263	0,057966	-0,01991	-0,02478	-0,02788	0,070439	0,084605
17,28	0,048574	0,054305	0,056776	-0,02091	-0,02286	-0,02859	0,069987	0,084133
18,36	0,048509	0,055915	0,055248	-0,02244	-0,02126	-0,02869	0,069996	0,084068
19,44	0,049236	0,057333	0,053571	-0,02428	-0,0201	-0,02827	0,070272	0,084346
20,52	0,050678	0,05833	0,052081	-0,0261	-0,01962	-0,0274	0,070964	0,085318
21,6	0,052174	0,058487	0,050537	-0,02745	-0,01966	-0,026	0,070813	0,085093
22,68	0,053703	0,05762	0,04912	-0,02834	-0,02025	-0,02412	0,07028	0,08426
23,76	0,055404	0,056297	0,048388	-0,02871	-0,02154	-0,02226	0,070077	0,084068
24,84	0,05691	0,05475	0,048638	-0,02856	-0,02323	-0,02079	0,070113	0,084165
25,92	0,058049	0,05303	0,049634	-0,02781	-0,02513	-0,01983	0,0706	0,084749
27	0,058585	0,051597	0,051267	-0,0267	-0,0268	-0,01963	0,071026	0,0853
28,08	0,057966	0,050029	0,05263	-0,02498	-0,02788	-0,01977	0,070564	0,08467
29,16	0,056776	0,048847	0,054305	-0,02305	-0,02859	-0,02063	0,070007	0,084151
30,24	0,055248	0,048448	0,055915	-0,02139	-0,02869	-0,02205	0,069973	0,084055
31,32	0,053571	0,048889	0,057333	-0,02016	-0,02827	-0,02387	0,070229	0,084297
32,4	0,052081	0,050159	0,05833	-0,01965	-0,0274	-0,02574	0,070844	0,085083
33,48	0,050537	0,051685	0,058487	-0,01961	-0,026	-0,02721	0,070972	0,085227
34,56	0,04912	0,053138	0,05762	-0,02015	-0,02412	-0,02817	0,070204	0,084346
35,64	0,048388	0,054857	0,056297	-0,02134	-0,02226	-0,02868	0,070022	0,084061
36	0,048412	0,055404	0,055761	-0,02188	-0,02175	-0,02871	0,069973	0,084073

Appendix V

Locked rotor measurement results for 10 poled rotor, results in ohm and Henries

Angle	Ra	Rb	Rc	La	Lb	Lc	Lab	Lac	Lba	Lbc	Lca	Lcb	Ld	Lq
0	3,546456	3,91056	3,91056	0,047893	0,05281	0,05281	-0,02116	-0,02134	-0,02095	-0,02592	-0,02112	-0,02592	0,06908	0,07873
1,5	3,597485	4,065946	3,858764	0,048582	0,054908	0,05211	-0,02309	-0,01994	-0,0229	-0,02556	-0,02006	-0,02592	0,06964	0,07992
3	3,699541	4,117741	3,674027	0,049908	0,055517	0,049535	-0,02481	-0,01939	-0,02447	-0,02447	-0,01939	-0,02481	0,06911	0,07997
4,5	3,829967	4,065946	3,57197	0,051599	0,054778	0,048123	-0,02566	-0,01986	-0,02568	-0,02285	-0,01989	-0,02303	0,06906	0,0796
6	3,962355	3,962355	3,546456	0,053351	0,053422	0,047815	-0,0262	-0,02089	-0,02602	-0,02106	-0,02075	-0,02127	0,06896	0,07949
7,5	4,01415	3,829967	3,597485	0,054008	0,051568	0,048402	-0,02565	-0,02246	-0,02563	-0,02001	-0,02265	-0,02004	0,06921	0,07892
9	4,065946	3,699541	3,699541	0,054746	0,049775	0,049775	-0,02443	-0,02425	-0,02441	-0,0197	-0,02441	-0,01988	0,06957	0,07899
10,5	4,065946	3,597485	3,829967	0,054705	0,048402	0,05153	-0,02282	-0,02565	-0,023	-0,02021	-0,02563	-0,02001	0,06942	0,07944
12	3,988253	3,597485	3,962355	0,05366	0,048374	0,053311	-0,0214	-0,02618	-0,02126	-0,02126	-0,02618	-0,02122	0,06973	0,07966
13,5	3,91056	3,648513	4,01415	0,052583	0,049089	0,054008	-0,0205	-0,02563	-0,02055	-0,02299	-0,02545	-0,02298	0,07059	0,07923
15	3,750569	3,750569	4,065946	0,050395	0,050432	0,054632	-0,02001	-0,02436	-0,02001	-0,02471	-0,02455	-0,0242	0,07042	0,07916
16,5	3,648513	3,91056	4,01415	0,049024	0,052545	0,053937	-0,02053	-0,02262	-0,02084	-0,02579	-0,02278	-0,02561	0,07055	0,07918
18	3,648513	4,01415	3,962355	0,049024	0,053976	0,053241	-0,02193	-0,02123	-0,02173	-0,02596	-0,02137	-0,02614	0,07062	0,07966
19,5	3,699541	4,065946	3,829967	0,049709	0,054632	0,051462	-0,02332	-0,02053	-0,02331	-0,02596	-0,02069	-0,02542	0,07079	0,0795
21	3,829967	4,065946	3,699541	0,051462	0,054632	0,049709	-0,02507	-0,02034	-0,0249	-0,02384	-0,02019	-0,02401	0,07085	0,07914
22,5	3,962355	4,01415	3,597485	0,053241	0,053937	0,048302	-0,02596	-0,02084	-0,02579	-0,0219	-0,02106	-0,0221	0,0703	0,07924
24	4,01415	3,962355	3,57197	0,053937	0,053241	0,047995	-0,02614	-0,02137	-0,02614	-0,02102	-0,02123	-0,02123	0,06943	0,07973
25,5	4,065946	3,829967	3,597485	0,054592	0,051462	0,048302	-0,02559	-0,02277	-0,02575	-0,01997	-0,02295	-0,02	0,06919	0,07939
27	4,091844	3,699541	3,674027	0,05494	0,049673	0,04933	-0,02453	-0,02418	-0,02469	-0,0193	-0,02434	-0,01947	0,06889	0,07925
28,5	4,065946	3,597485	3,778558	0,054592	0,048302	0,050704	-0,02294	-0,02524	-0,02313	-0,01982	-0,0254	-0,0198	0,06892	0,07892
30	3,988253	3,546456	3,962355	0,053549	0,047617	0,053201	-0,02136	-0,02612	-0,02139	-0,02069	-0,02612	-0,02083	0,06892	0,0795
31,5	3,91056	3,597485	4,01415	0,052506	0,048302	0,053897	-0,02012	-0,02612	-0,02	-0,02243	-0,02577	-0,02224	0,06933	0,07936
33	3,750569	3,674027	4,091844	0,050358	0,04933	0,05494	-0,01982	-0,02469	-0,01965	-0,024	-0,02471	-0,02418	0,06958	0,07919
34,5	3,648513	3,829967	4,065946	0,048987	0,051424	0,054592	-0,02	-0,02347	-0,01997	-0,0254	-0,0233	-0,02506	0,06989	0,07918
36	3,597485	3,962355	3,962355	0,048302	0,053201	0,053201	-0,02121	-0,02121	-0,02118	-0,02612	-0,02136	-0,02612	0,06955	0,07932

Appendix VI

Inductance values fom FEM calculation for the 14 poled rotor, in Henries

Angle	La	Lb	Lc	Lab	Lac	Lbc	Ld	Lq
0	0,056047	0,061087	0,061043	-0,0255	-0,025483	-0,030482	0,081722	0,091752
0,714286	0,056382	0,061878	0,060395	-0,026426	-0,024883	-0,030424	0,082111	0,091923
1,428571	0,057254	0,062597	0,05972	-0,027545	-0,024641	-0,029986	0,082773	0,091947
2,142857	0,058591	0,062839	0,058676	-0,028885	-0,024646	-0,028937	0,083204	0,091801
2,857143	0,059732	0,062554	0,057302	-0,029987	-0,024659	-0,027556	0,082727	0,091937
3,571429	0,060375	0,061959	0,05631	-0,030422	-0,024865	-0,026386	0,082062	0,091844
4,285714	0,061024	0,061032	0,056059	-0,030448	-0,0255	-0,025494	0,081739	0,091716
5	0,061949	0,060326	0,056352	-0,030432	-0,026438	-0,024884	0,082107	0,09189
5,714286	0,062628	0,05975	0,05726	-0,029994	-0,027552	-0,024645	0,082793	0,091941
6,428571	0,062829	0,058704	0,0586	-0,028896	-0,028881	-0,024656	0,083365	0,09187
7,142857	0,062557	0,057282	0,059788	-0,027523	-0,029962	-0,024674	0,082879	0,092051
7,857143	0,061876	0,05636	0,060403	-0,0264	-0,030399	-0,02488	0,082048	0,091822
8,571429	0,061043	0,056047	0,061087	-0,025492	-0,030482	-0,025503	0,081768	0,091669
9,285714	0,060395	0,056382	0,061878	-0,02488	-0,030424	-0,026393	0,081998	0,091907
10	0,05972	0,057254	0,062597	-0,024653	-0,029986	-0,027551	0,082888	0,091938
10,71429	0,058676	0,058591	0,062839	-0,024659	-0,028937	-0,028886	0,083273	0,091806
11,42857	0,057302	0,059732	0,062554	-0,024672	-0,027556	-0,029967	0,082734	0,091949
12,14286	0,05631	0,060375	0,061959	-0,024867	-0,026386	-0,03045	0,082085	0,091908
12,85714	0,056059	0,061024	0,061032	-0,0255	-0,025494	-0,030463	0,081746	0,091759
13,57143	0,056352	0,061949	0,060326	-0,026409	-0,024884	-0,030403	0,082177	0,091917
14,28571	0,05726	0,062628	0,05975	-0,027549	-0,024645	-0,030007	0,082895	0,091911
15	0,0586	0,062829	0,058704	-0,028895	-0,024656	-0,028936	0,083305	0,091741
15,71429	0,059788	0,062557	0,057282	-0,030024	-0,024674	-0,027549	0,082787	0,091903
16,42857	0,060403	0,061876	0,05636	-0,030433	-0,02488	-0,026402	0,082014	0,091851
17,14286	0,061087	0,061043	0,056047	-0,030492	-0,025503	-0,025483	0,081748	0,091708
17,85714	0,061878	0,060395	0,056382	-0,0304	-0,026393	-0,024883	0,082281	0,091878
18,57143	0,062597	0,05972	0,057254	-0,029972	-0,027551	-0,024641	0,082869	0,091966
19,28571	0,062839	0,058676	0,058591	-0,028901	-0,028886	-0,024646	0,083431	0,091839
20	0,062554	0,057302	0,059732	-0,027523	-0,029967	-0,024659	0,082785	0,091914
20,71429	0,061959	0,05631	0,060375	-0,026415	-0,03045	-0,024865	0,082066	0,091819
21,42857	0,061032	0,056059	0,061024	-0,025488	-0,030463	-0,0255	0,081658	0,091728
22,14286	0,060326	0,056352	0,061949	-0,024864	-0,030403	-0,026438	0,081974	0,091904
22,85714	0,05975	0,05726	0,062628	-0,024657	-0,030007	-0,027552	0,082758	0,091924
23,57143	0,058704	0,0586	0,062829	-0,024686	-0,028936	-0,028881	0,083262	0,091776
24,28571	0,057282	0,059788	0,062557	-0,024658	-0,027549	-0,029962	0,082773	0,091941
25	0,05636	0,060403	0,061876	-0,024884	-0,026402	-0,030399	0,082126	0,091908
25,71429	0,056136	0,061087	0,061043	-0,025541	-0,025523	-0,030482	0,08188	0,091825

Appendix VII

Locked rotor measurement results for 14 poled rotor, results in ohm and Henries

Angle	Ra	Rb	Rc	La	Lb	Lc	Lab	Lac	Lba	Lbc	Lca	Lcb	Ld	Lq
0,00	6,29324	6,86981	6,93851151	0,055878	0,06123	0,061862	-0,02574	-0,02574	-0,02514	-0,03104	-0,02545	-0,03073	0,081496	0,092428
1,07	6,29324	6,93851	6,6774586	0,056049	0,061809	0,059465	-0,02672	-0,02462	-0,02677	-0,0302	-0,02476	-0,03026	0,081466	0,091192
2,14	6,47511	6,93851	6,48361846	0,057651	0,06177	0,057733	-0,02872	-0,02445	-0,02832	-0,02894	-0,02423	-0,02877	0,082027	0,090551
3,21	6,67746	6,93851	6,29323976	0,059415	0,061738	0,056002	-0,02993	-0,02443	-0,03017	-0,02737	-0,02459	-0,02729	0,081497	0,091201
4,29	6,80679	6,93851	6,29323976	0,060553	0,061725	0,055978	-0,0305	-0,02527	-0,03079	-0,02612	-0,02549	-0,02549	0,081606	0,091782
5,36	7,07591	6,67746	6,29323976	0,062927	0,059377	0,055978	-0,03078	-0,02673	-0,03083	-0,02411	-0,02668	-0,02428	0,080844	0,092481
6,43	7,27941	6,54256	6,41677704	0,06473	0,058178	0,057053	-0,03009	-0,02914	-0,03021	-0,0235	-0,02903	-0,02329	0,081009	0,09405
7,50	7,00721	6,29324	6,54256045	0,062296	0,055943	0,058165	-0,02766	-0,02952	-0,02757	-0,02397	-0,0299	-0,0241	0,080814	0,091033
8,57	6,93851	6,29324	6,81235676	0,061673	0,055937	0,060545	-0,02579	-0,03107	-0,02577	-0,02547	-0,03051	-0,02501	0,08141	0,091897
9,64	6,6173	6,81236	6,81235676	0,058805	0,060532	0,060539	-0,02448	-0,02962	-0,02592	-0,02958	-0,02928	-0,02623	0,085026	0,08993
10,71	6,54256	6,41678	6,93851151	0,058116	0,056987	0,061614	-0,02469	-0,02866	-0,02447	-0,0284	-0,02857	-0,02826	0,082133	0,090026
11,79	6,40766	6,80112	7,27807657	0,056894	0,060381	0,064616	-0,02468	-0,02804	-0,02483	-0,03073	-0,02809	-0,03129	0,082736	0,09441
12,86	6,52632	6,07042	6,18283204	0,058144	0,053894	0,055084	-0,02678	-0,02647	-0,02599	-0,02324	-0,02638	-0,02407	0,084249	0,078143
13,93	6,64946	6,85411	6,92943817	0,059222	0,061051	0,061729	-0,02823	-0,02601	-0,03074	-0,02562	-0,02538	-0,03077	0,086486	0,09043
15,00	6,78945	7,3452	6,78944952	0,060469	0,065425	0,060475	-0,03013	-0,02538	-0,02992	-0,02959	-0,02538	-0,03013	0,085848	0,095243
16,07	7,34666	7,64198	6,77733512	0,065431	0,068069	0,060361	-0,03428	-0,02571	-0,0343	-0,02959	-0,02586	-0,02974	0,087402	0,101667
17,14	7,56779	7,49359	6,77733512	0,067401	0,06674	0,060361	-0,0343	-0,02791	-0,0343	-0,02757	-0,0278	-0,02716	0,087979	0,101365
18,21	7,58246	7,12556	6,76474564	0,067532	0,063462	0,060249	-0,03325	-0,02919	-0,03329	-0,02597	-0,02967	-0,02538	0,086717	0,099694
19,29	8,2087	7,19682	6,98296325	0,073109	0,064097	0,062192	-0,03362	-0,03362	-0,03329	-0,02555	-0,03099	-0,02538	0,088615	0,105135
20,36	6,75826	6,76475	6,90004056	0,060191	0,060249	0,061454	-0,02763	-0,0273	-0,03066	-0,02571	-0,0269	-0,02858	0,088472	0,088382
21,43	8,04419	8,12977	8,66985886	0,071644	0,072406	0,077208	-0,02796	-0,03822	-0,02897	-0,03827	-0,04231	-0,02909	0,101085	0,114697
22,50	7,49511	7,80583	8,05083662	0,066739	0,10174	0,071695	-0,0271	-0,03362	-0,03081	-0,03362	-0,03469	-0,03147	0,117616	0,106269
23,57	7,26798	7,19227	7,88311085	0,064717	0,093743	0,070194	-0,0271	-0,03224	-0,0271	-0,03224	-0,03222	-0,03222	0,106334	0,10714
24,64	7,19227	7,57397	9,09759572	0,064043	0,098718	0,081009	-0,02641	-0,03224	-0,02766	-0,03502	-0,03402	-0,04082	0,102784	0,125119
25,71	7,18993	8,49109	8,49108934	0,064022	0,110671	0,075608	-0,02946	-0,02911	-0,03025	-0,03959	-0,03025	-0,03922	0,100307	0,132524